

MonarchRT: Efficient Attention for Real-Time Video Generation

Krish Agarwal¹, Zhuoming Chen¹, Cheng Luo, Yongqi Chen³, Haizhong Zheng¹, Xun Huang³, Atri Rudra², Beidi Chen¹

{krisha2,zhuominc,haizhonz,beidic}@andrew.cmu.edu

wdlctc@gmail.com, yongqichcd@gmail.com, xunhuang1995@gmail.com, atri@buffalo.edu

¹Carnegie Mellon University

²University at Buffalo

³Morpheus AI

Real-time video generation with Diffusion Transformers is bottlenecked by the quadratic cost of 3D self-attention, especially in real-time regimes that are both few-step and autoregressive, where errors compound across time and each denoising step must carry substantially more information. In this setting, we find that prior sparse-attention approximations break down, despite showing strong results for bidirectional, many-step diffusion. Specifically, we observe that video attention is not reliably sparse, but instead combines pronounced periodic structure driven by spatiotemporal position with dynamic, sparse semantic correspondences and dense mixing, exceeding the representational capacity of even oracle top- k attention. Building on this insight, we propose **MonarchRT**, a structured attention parameterization for video diffusion models that factorizes attention using Monarch matrices. Through appropriately aligned block structure and our extended *tiled Monarch parameterization*, we achieve high expressivity while preserving computational efficiency. We further overcome the overhead of parameterization through finetuning, with custom Triton kernels. We first validate the high efficacy of MONARCHRT over existing sparse baselines designed only for bidirectional models. We further observe that MONARCHRT attains up to 95% *attention sparsity* with no loss in quality when applied to the state-of-the-art model Self-Forcing, making Monarch-RT a pioneering work on highly-capable sparse attention parameterization for real-time video generation. Our optimized implementation outperforms FlashAttention-2, FlashAttention-3, and FlashAttention-4 kernels on Nvidia RTX 5090, H100, and B200 GPUs respectively, providing kernel speedups in the range of 1.4-11.8 \times . This enables us, for the first time, to achieve true real-time video generation with Self-Forcing at 16 FPS on a single RTX 5090.



Github: <https://github.com/Infini-AI-Lab/MonarchRT>

Website: <https://infini-ai-lab.github.io/MonarchRT>

1 Introduction

With the common understanding that substantial redundancy exists in 3D attention, many approximation algorithms have been proposed to reduce its computational cost. However, we found that two key properties critical to real-time video generation (Zhang et al., 2025b), namely **auto-regressiveness** (Huang et al., 2025; Teng et al., 2025; Yin et al., 2025) and the use of **fewer diffusion steps** (Yin et al., 2024b,a; Liu et al., 2024, 2025), can significantly amplify approximation difficulties. Auto-regressive generation accumulates errors over time, while shortening the diffusion process compresses computation, causing each diffusion step to process substantially more information. Critically, these features are key in the design of real-time, *interactive* video generation models, including Genie 3 (Ball et al., 2025), WorldPlay (Sun et al., 2025), and LingBot-World (Team et al., 2026).

Prior efficient approximations for 3D attention are fundamentally constrained by their **limited expressiveness**, which leads to substantial degradation in generated video quality. *Sparse attention* methods capture **positional patterns** by restricting attention to temporally and spatially local neighborhoods (Li et al., 2025; Xi et al., 2025; Zhang et al., 2025d), or capture **semantic patterns** by attending to a small subset of tokens selected via clustering or retrieval-based strategies (Zhang et al., 2025c; Yang et al., 2025; Zhang et al., 2025a). The former class weakens the inherent ability of DiTs to model long-range semantic dependencies, effectively regressing

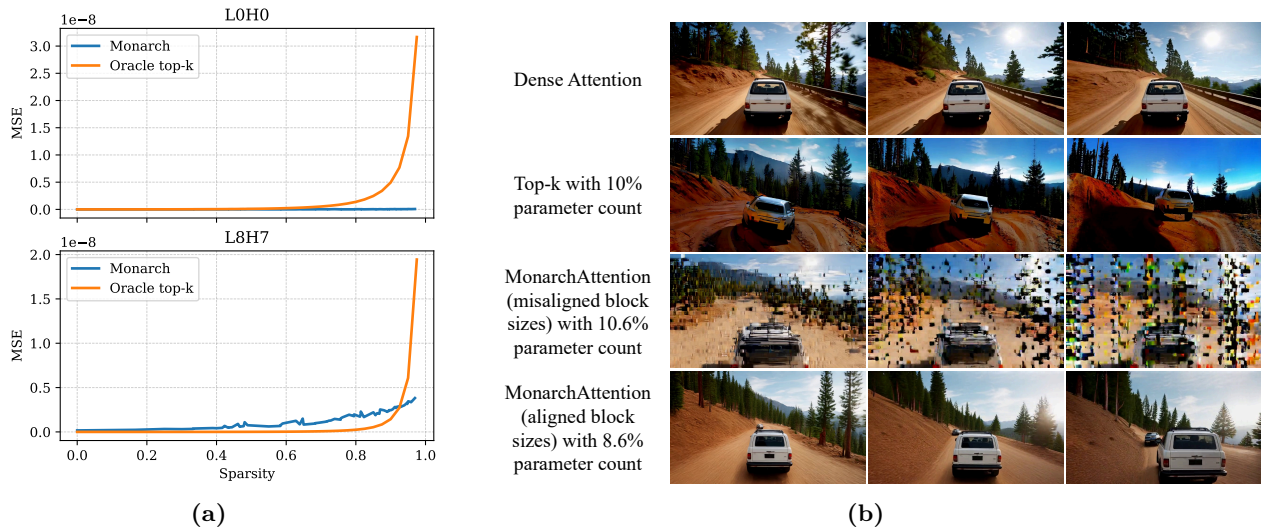


Figure 1 Left: MSE of oracle top- k and Monarch parameterizations of an attention map compared to the original dense attention map for varying levels of sparsity. Results shown for two different layers/heads on Self-Forcing. Monarch incurs much lower error for high levels of sparsity. **Right:** Example generations on the same prompt on Self-Forcing. First row shows exact top- k with 10% density still produces poor quality output. Third row shows that using inference-only MonarchAttention (with aligned block sizes) produces higher output quality with a lower parameter count of 8.6%. Second row shows that, although the parameter count is increased to 10.6%, inference-only MonarchAttention with misaligned block sizes incurs pixel-level permutation effects. Parameter count refers to the number of parameters used to estimate the full attention map.

toward convolution-based architectures (Çiçek et al., 2016; Ronneberger et al., 2015), whose representational limitations are well known. The latter class, while more flexible, is highly parameter-inefficient when **dense mixing** is required, as evidenced by the failure of oracle top- k attention even with 10% of the FLOPs of full attention (Figure 1b). *Low-rank and linear attention* methods similarly struggle to represent long-range semantic patterns empirically (Zhou et al., 2025; He and Garner, 2025) and often requiring substantial retraining to adapt from DiTs (Zhang et al., 2025a). As a result, to preserve video quality, existing approaches typically retain more than 40% of the FLOPs of full attention (Zhang et al., 2025a; Yang et al., 2025; Xi et al., 2025). While such compromises can be effective for many-step diffusion models such as Wan 2.1 (Wan et al., 2025), which exploit redundancy across approximately 50 diffusion steps, they are fundamentally incompatible with state-of-the-art real-time video generation systems that operate with far fewer steps (Huang et al., 2025; Zhang et al., 2025b).

Therefore, to preserve the strengths of DiTs while remaining viable for real-time video generation, an ideal attention approximation must simultaneously capture three critical patterns: **positional patterns**, **semantic patterns**, and **dense mixing**. This naturally raises the question of whether there exists an approach that is substantially more computationally efficient than full attention while retaining strong expressive power.

Beyond sparse and low-rank methodologies, Monarch (Dao et al., 2022a, 2021; Sa et al., 2017) introduces a unifying class of structured matrices that can efficiently represent a broad family of linear operators, including sparse and low-rank matrices as well as structured transforms such as FFT and Hadamard. More recently, MonarchAttention (Yaras et al., 2025), which employs an iterative optimization procedure to efficiently obtain Monarch factors, demonstrates that attention matrices themselves can be effectively approximated using Monarch parameterizations. Our empirical analysis (Figure 1a) further reveals that Monarch parameterizations recover 3D attention matrices significantly better than oracle top- k or low-rank approximations, pointing to a promising direction for accelerating real-time video generation without sacrificing expressiveness.

However, leveraging Monarch parameterizations to approximate 3D attention in practical real-time video generation systems introduces several non-trivial technical challenges. First (Shape Alignment), unlike Monarch in MLPs (Dao et al., 2022a; Fu et al., 2023), where the semantics of input and output channels can be learned implicitly during training, the rows and columns of 3D attention matrices are explicitly tied to

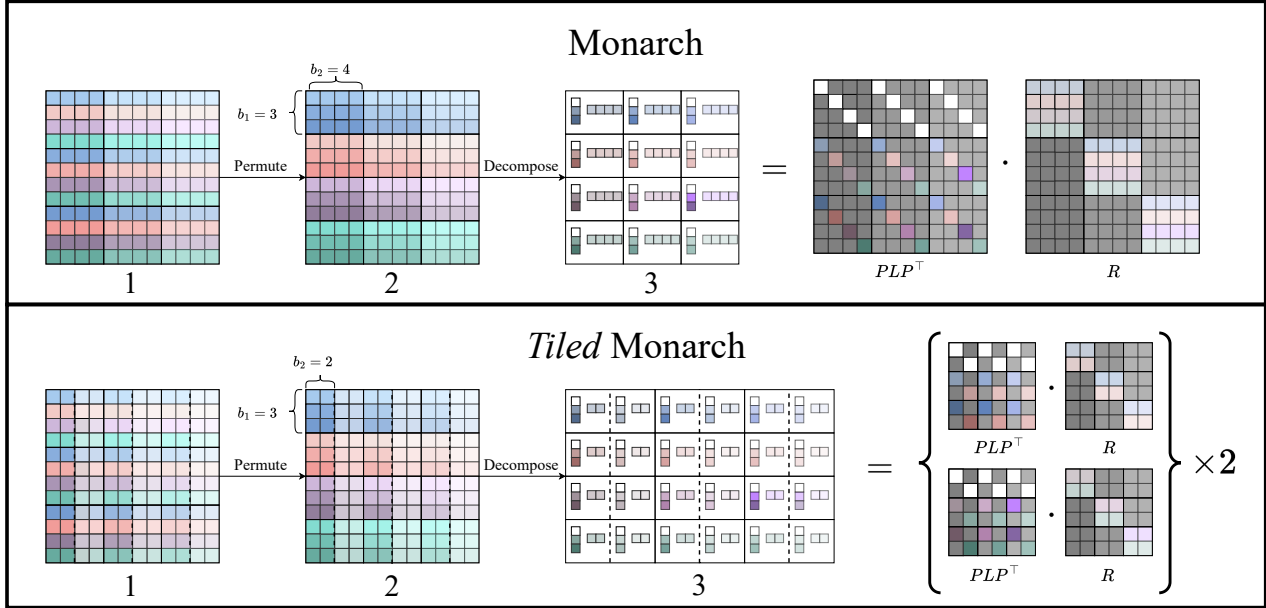


Figure 2 Illustration of Regular and Tiled Monarch Parameterization. Top: An example of Monarch parameterization applied to a 12×12 matrix with block size $(b_1, b_2) = (3, 4)$. Bottom: An example of *tiled* Monarch parameterization applied with block size $(b_1, b_2) = (3, 2)$. (1) The original matrix is first permuted to expose an implicit block-wise low-rank structure. (2) After permutation, the matrix is reorganized into blocks of size $b_1 \times b_2$, where each block corresponds to a group of rows and columns. (3) Each block is then independently decomposed into low-rank factors. Overall, Monarch represents the matrix as $PLP^T R$, where P denotes a permutation matrix, PLP^T is a block-wise diagonal matrix, and R is a block-diagonal matrix. The tiled Monarch parameterization has $2 \times$ the parameter count and is strictly more expressive than the regular Monarch parameterization.

physical pixel patches in a video. Consequently, when the structural assumptions of Monarch parameterizations (e.g., block sizes) are misaligned with the spatial-temporal layout of pixel patches, the approximation quality can degrade dramatically, often leading to severe artifacts or even complete collapse of the generated videos. Second (Limited Flexibility), although Monarch allows adjusting computational cost by varying block sizes, we observe a systematic issue in which the approximation error does not reliably decrease as more FLOPs are allocated. This lack of monotonic refinement fundamentally limits Monarch’s ability to progressively improve approximation quality, in sharp contrast to sparse-attention-based methods whose accuracy typically scales with increased computation. Third (High Runtime Overhead), the iterative refinement strategy adopted by MonarchAttention (Yaras et al., 2025) requires multiple refinement steps to achieve high-quality approximations, rendering it computationally prohibitive for real-time video generation systems with strict latency constraints.

To address these challenges, we introduce MONARCHRT, a unified framework for applying Monarch parameterizations to video generation. MONARCHRT first provides a factorization structure that is explicitly compatible with 3D attention, and further enables *arbitrarily accurate* matrix approximations through our proposed *Tiled Monarch Parameterizations* (illustrated in Figure 2 Bottom). In addition, by finetuning MonarchAttention, we substantially reduce the number of iterative refinement steps required during inference. These components make Monarch parameterization both accurate and efficient for real-time video generation.

In summary, our contributions are as follows:

- In Sections 3.1 to 3.3, we analyze the structural patterns of 3D video attention, explaining why existing sparse- and low-rank-based methods fail to capture them, and why Monarch provides a principled and expressive parameterization for 3D attention.
- In Section 3.4, we identify the key practical challenges in applying Monarch parameterizations to video models, including *shape misalignment*, *limited flexibility*, and *parameterization overhead*.
- In Sections 4.1 and 4.2, we introduce *Tiled Monarch Parameterization*, together with a simple yet crucial block-alignment strategy. This formulation generalizes the original Monarch parameterization and enables

arbitrarily accurate approximations of 3D attention matrices.

- In Section 4.3, we demonstrate how training can be leveraged to minimize inference-time cost by reducing the number of iterative refinement steps. We further provide an efficient Triton implementation that supports both forward and backward passes of Monarch attention.

In Section 5, we conduct comprehensive evaluations of MONARCHRT across multiple video generation settings. We benchmark our method against existing sparse-attention-based approaches on auto-regressive video models (e.g., Self-Forcing), demonstrating that MONARCHRT achieves the highest visual quality under real-time generation constraints. While prior sparse attention methods fail to maintain visual fidelity beyond 85% sparsity, MONARCHRT preserves high generation quality even when reducing attention computation by 95%. We further apply MONARCHRT to bidirectional video diffusion models (e.g., Wan 2.1-1.3B (Wan et al., 2025)) and compare it against additional sparse/dense baselines. MONARCHRT consistently achieves comparable generation quality while significantly reducing computational cost. Using our optimized kernel implementation, MONARCHRT obtains up to a $5.6\times$ speedup over FA-3 (Shah et al., 2024) on H100 and $11.8\times$ over FA-2 (Dao et al., 2022b; Dao, 2023) on RTX 5090. Notably, with MONARCHRT we are able to achieve true real-time generation at 16 FPS with Self-Forcing on RTX 5090.

2 Background

In this section, we first discuss related work on Monarch parameterizations and MonarchAttention. Then we provide a visualization to illustrate the Monarch parameterization process. Finally, we formally present the attention approximation problem.

2.1 Monarch

Monarch Parameterization. Monarch parameterization (Dao et al., 2022a) represents an $N \times N$ matrix \mathbf{M} , with $N = b_1 b_2$, using a structured factorization defined by two block sizes b_1 and b_2 . Concretely, \mathbf{M} is expressed as

$$\mathbf{M} = \mathbf{P} \mathbf{L} \mathbf{P}^\top \mathbf{R},$$

where \mathbf{P} is a fixed permutation matrix that reshapes a length- N vector into a $b_1 \times b_2$ matrix, transposes it, and flattens it back. This permutation exposes an implicit block-wise structure in \mathbf{M} , as illustrated in Figure 2. After permutation, \mathbf{L} is block-diagonal with b_2 blocks of size $b_1 \times b_1$, each operating independently on a group of rows, while \mathbf{R} is block-diagonal with b_1 blocks of size $b_2 \times b_2$, each operating on a group of columns. Intuitively, Monarch assumes that, after permutation, the matrix can be decomposed into independent low-rank blocks along the two axes. Equivalently, Monarch can be interpreted as a block-wise rank-1 structure under permutation. Specifically, \mathbf{M} can be viewed as a 4D tensor of shape $b_1 \times b_2 \times b_1 \times b_2$, with entries defined as

$$M_{\ell j k i} = \mathbf{L}_{j \ell k} \mathbf{R}_{k j i}.$$

This perspective leads to an efficient projection algorithm: given an arbitrary $N \times N$ matrix, one first permutes it, reshapes it into the 4D form, and then performs independent rank-1 projections on each post-permutation 2D slice (along the ℓ and i dimensions) to populate \mathbf{L} and \mathbf{R} . The class of Monarch matrices strictly generalizes butterfly matrices. Since sparse matrices can be represented as products of butterfly matrices (Dao et al., 2021), the same representational guarantees extend to Monarch parameterizations. An example with $N = 12$ and $(b_1, b_2) = (3, 4)$ is visualized in Figure 2 Top.

MonarchAttention aims to approximate the full attention matrix $\mathbf{A} = \text{softmax}(\mathbf{Q} \mathbf{K}^\top) \in \mathbb{R}^{N \times N}$ using Monarch parameterization with factors $\mathbf{L} \in \mathbb{R}^{b_2 \times b_1 \times b_1}$ and $\mathbf{R} \in \mathbb{R}^{b_1 \times b_2 \times b_2}$, where block sizes b_1 and b_2 satisfy $N = b_1 b_2$ (Yaras et al., 2025). A direct approach would require explicitly forming \mathbf{A} and projecting it onto the Monarch structure via SVD on each permuted block, which is computationally prohibitive. To avoid materializing the full attention matrix, MonarchAttention proposes an iterative refinement algorithm that directly optimizes the Monarch factors. Leveraging an alternative variational formulation of softmax (Blondel et al., 2019), the attention matrix can be expressed as

$$\mathbf{A} = \arg \max_{\mathbf{A}_i \in \Delta^N} \langle \mathbf{A}, \mathbf{Q} \mathbf{K}^\top \rangle + H(\mathbf{A}),$$

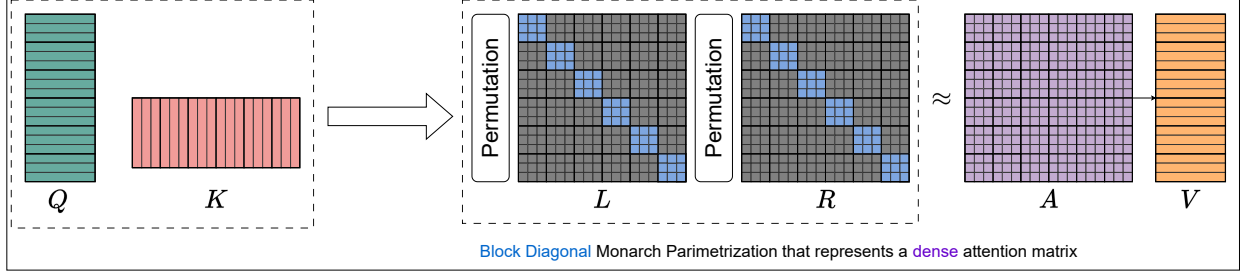


Figure 3 Overview of the MonarchAttention pipeline. Given query and key matrices (Q, K), MonarchAttention iteratively refines the Monarch factors L and R , each composed of sparse block-diagonal matrices. At each iteration, one factor is updated while the other is held fixed, without explicitly materializing the full attention matrix. Despite the highly structured and sparse parameterization of L and R , the resulting attention matrix $A \approx PLP^T R$ is dense, highlighting the strong expressiveness of Monarch parameterization. Algorithmic details are provided in Appendix A.

where $H(\cdot)$ denotes the entropy. By constraining A to lie in the Monarch family, it can be interpreted as a $b_1 \times b_2 \times b_1 \times b_2$ tensor with entries $A_{\ell j k i} = L_{j \ell k} R_{k j i}$. This formulation allows the objective to be optimized directly over L and R . Through careful manipulation of the objective and by imposing slightly stronger constraints on the factors, MonarchAttention enables alternating maximization: updating R while holding L fixed, and vice versa. After a reasonable number of iterations, the algorithm produces Monarch factors that can be applied sequentially to the value matrix V to compute the attention output, without ever constructing the dense attention matrix explicitly. The pipeline is illustrated in Figure 3. Additional algorithmic details are provided in Section A.

2.2 Problem Formulation

Given query, key, and value matrices $Q, K, V \in \mathbb{R}^{n \times d}$, the attention output is

$$\text{Attn}(Q, K, V) = \text{softmax}(QK^\top)V,$$

where the softmax is applied row-wise. We denote the attention matrix by $A = \text{softmax}(QK^\top) \in \mathbb{R}^{n \times n}$. The goal of attention parameterization is to reduce the quadratic cost of computing A while preserving approximation quality.

Formally, given an approximation procedure $f(Q, K)$, we seek to balance the approximation error

$$\mathbb{E} \left[\|f(Q, K) - A\|_F^2 \right],$$

and the computational cost $\mathcal{C}(f(\cdot))$.

We consider three representative parameterization families, each imposing a distinct structural constraint on A :

1. Sparse.

$$A_s = \arg \min_{A' \in \mathbb{R}^{n \times n} : \text{NNZ}(A')} \|A' - A\|_F^2.$$

2. Low-rank.

$$A_\ell = \arg \min_{\bar{Q}, \bar{K} \in \mathbb{R}^{n \times \bar{n}}} \|\bar{Q}\bar{K}^\top - A\|_F^2, \quad \bar{n} < n.$$

3. Monarch.

$$A_m = \arg \min_{A' \in \mathcal{M}} \|A' - A\|_F^2,$$

where \mathcal{M} denotes the family of Monarch matrices.

An ideal parameterization achieves low approximation error with minimal computational cost, which is ultimately governed by the structural properties of A .



Figure 4 **Left:** Percent of key-value tokens that fall under the top- p threshold per head in Self-Forcing, averaged across all query tokens for several decoding iterations, on the first denoising iteration. Results shown for 5 randomly sampled heads/layers. **textbf{Right:}** Example generations on the same prompt on Self-Forcing using MONARCHRT with 10 and 1 iterations of iterative refinement. 10 iterations has much higher quality but is practically inefficient, so we recover the accuracy of 1 iteration with training.

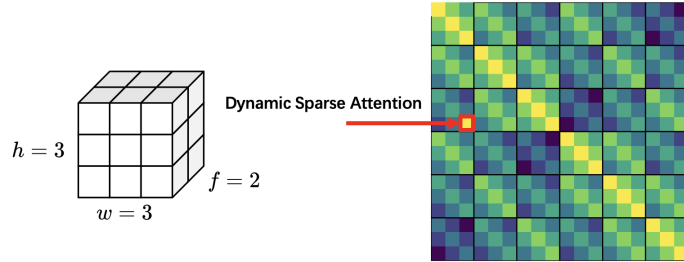


Figure 5 An illustration of our modeling of the 3D attention map in Equation (1). **Left:** the shape of the video. **Right:** an example attention map. The periodic diagonal bands arise from spatiotemporal positional structure, while the large activation at position (8, 2) reflects a semantic relationship that is independent of position, requiring dynamic (retrieval-based) sparse attention to capture.

3 Observations and Analysis

In this section, we present our core argument that, in principle, Monarch parameterization provides a fundamentally stronger approximation than sparse parameterization for modeling 3D attention. We further identify three key challenges that arise in practice, each of which limits its flexibility and achievable accuracy.

3.1 Approximation Error Analysis

Failure of oracle top- k attention. In Figures 1a and 1b, we show that oracle top- k attention incurs large errors on approximating the attention map for high sparsity levels, leading to end-to-end quality degradation (the example car front exhibits severe geometric distortion), even with a 10% computation budget (which is reasonably high for an oracle approximation). We attribute this to the 3D attention map being less sparse than expected. As illustrated in Figure 4a, for certain attention heads, more than 48% \sim 84% tokens are required to recover 95% attention score. For non-oracle sparse parameterizations, such as those based on position or block top- k , the situation will become even worse, as such methods are not guaranteed to retrieve the keys producing the highest attention scores.

3.2 Rethinking the Structure of 3D Attention Maps

The failure of sparse parameterization stems from the incorrect assumption that the attention map is inherently sparse. 3D attention does not simply exhibit sparsity; instead, it reveals pronounced *periodic structure* driven by spatiotemporal position, indicating that dense and repeating interactions are fundamental rather than exceptional. Inspired by Li et al. (2025), we informally model the attention map as

$$\begin{aligned} \mathbf{A}_{(f_0, h_0, w_0), (f_1, h_1, w_1)} &= \mathbf{D}_{(f_0, h_0, w_0), (f_1, h_1, w_1)} + \mathbf{S}_{(f_0, h_0, w_0), (f_1, h_1, w_1)} + \epsilon, \\ \mathbf{D}_{(f_0, h_0, w_0), (f_1, h_1, w_1)} &= d_w(w_0, w_1) d_h(h_0, h_1) d_t(f_0, f_1). \end{aligned} \quad (1)$$

Here, \mathbf{D} captures the *positional* component of attention, modeled as the separable product of three distance

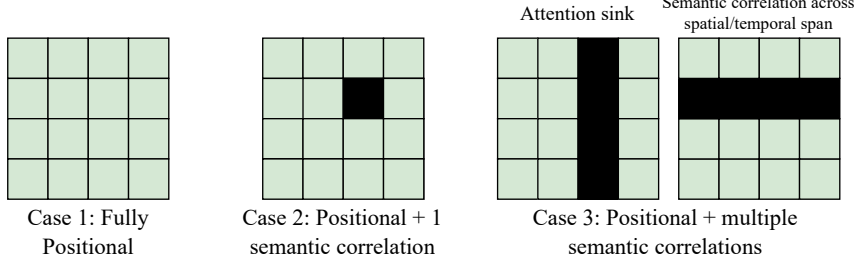


Figure 6 Illustration of several representative cases regarding occurrences of sparse, semantic correlations from a per-block ($\tilde{A}_{[i,j]}$) view of the full Monarch-parameterized attention map (\mathbf{A}).

functions along the spatial width (d_w), spatial height (d_h), and temporal (d_t) dimensions. Each distance function $d(\cdot, \cdot) \leq 1$ is monotonically decreasing, reflecting the empirical observation that attention scores induced by positional structure decay smoothly as tokens become farther apart. \mathbf{S} represents the *semantic* component, which models long-range relationships independent of positional proximity; most entries of \mathbf{S} are 0 due to the sparsity of meaningful semantic correspondence, the others are 1. ϵ denotes residual noise or modeling error. For simplicity, we omit the normalization here. This modeling immediately leads to Theorem 3.1.

Theorem 3.1. (informal) *The 3D attention matrix $\mathbf{A} \in \mathbb{R}^{fhw \times fhw}$ defined above admits a structural decomposition*

$$\mathbf{A} = \mathbf{P}\mathbf{D}' + \mathbf{S} + \epsilon$$

where \mathbf{P} is a permutation matrix, \mathbf{D}' is blockwise rank-1 with block sizes (b_1, b_2) , which satisfies $b_1 b_2 = fhw$ and \mathbf{S} is a sparse matrix.

Naively combining low-rank and sparse parameterization (Zhang et al., 2025a; Chen et al., 2021; Dong et al., 2024) is not sufficient, because a matrix that is low-rank within each local block can still become full-rank when viewed globally. We formally present Theorem 3.1 in Appendix B.1.

3.3 Monarch Well-Represents 3D Attention Maps

In this section, we discuss the intuition that Monarch parameterization could effectively represent the 3D attention map, i.e., $\mathbf{A} = \mathbf{P}\mathbf{D}' + \mathbf{S} + \epsilon$. We consider each block

$$\tilde{\mathbf{A}}_{[i,j]} = \mathbf{D}'_{[i,j]} + \tilde{\mathbf{S}}_{[i,j]} + \epsilon \in \mathbb{R}^{b_1 \times b_2},$$

where $\tilde{\mathbf{A}} = \mathbf{P}^\top \mathbf{A}$, $\tilde{\mathbf{S}} = \mathbf{P}^\top \mathbf{S}$, $[i, j]$ indexes the block positions in the partitioned attention matrix (i.e. $\tilde{\mathbf{A}}_{[i,j]} = \tilde{\mathbf{A}}_{[ib_1:(i+1)b_1, jb_2:(j+1)b_2]}$), and b_1, b_2 denote the block sizes. We now intuitively analyze three representative cases, also illustrated in Figure 6.

Case 1. If $\text{NNZ}(\tilde{\mathbf{S}}_{[i,j]}) = 0$, the block is entirely governed by the positional term. As the positional structure factorizes along the three dimensions, $\tilde{\mathbf{A}}_{[i,j]}$ reduces to a rank-1 matrix.

Case 2. When $\text{NNZ}(\tilde{\mathbf{S}}_{[i,j]}) = 1$ and the magnitude of $D_{[i,j]}$ is negligible, the block is dominated by a single semantic interaction between two distant tokens. In this situation, $\tilde{\mathbf{A}}_{[i,j]}$ is effectively determined by the single nonzero entry in $\tilde{\mathbf{S}}_{[i,j]}$, and the remaining entries can be approximated as zero. Consequently, $\tilde{\mathbf{A}}_{[i,j]}$ is also rank-1.

Case 3. When $\text{NNZ}(\tilde{\mathbf{S}}_{[i,j]}) > 1$ but all nonzero entries lie within a single row or a single column, while others are negligible the block corresponds to multiple semantic connections originating from (or pointing to) the same token. This pattern includes the common attention-sink phenomenon. Since all semantic interactions are confined to one row or column, $\tilde{\mathbf{A}}_{[i,j]}$ remains rank-1.

Since the number of strong semantic interactions (the nonzero entries of \mathbf{S}) is limited, an appropriate permutation \mathbf{P} and block sizes (b_1, b_2) can ideally prevent multiple semantic entries from falling into the same block or from mixing with strong positional interactions (i.e., from falling out of the listed 3 cases). Therefore, the

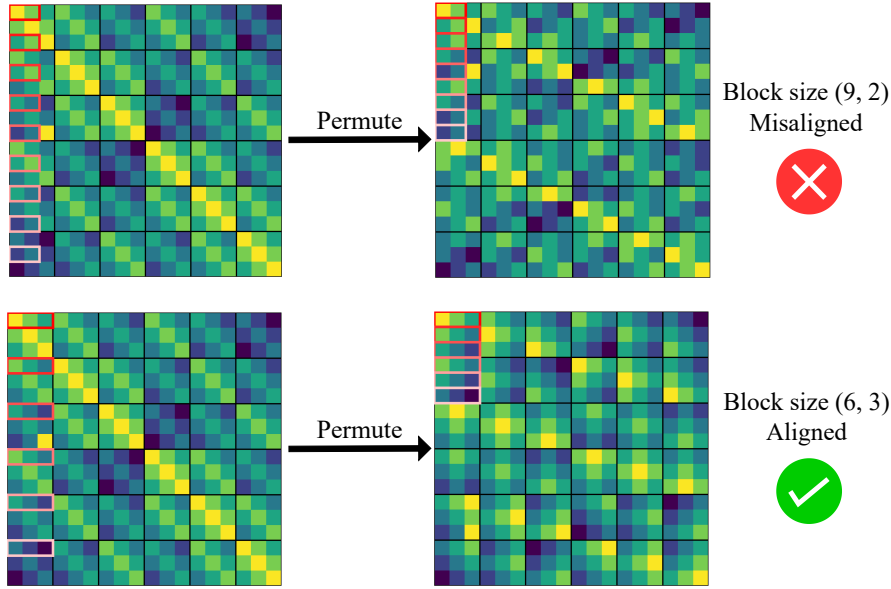


Figure 7 The comparison of two Monarch factorizations. The attention map is the same as Figure 5. **Top:** By selecting misaligned block sizes, most of the blocks are obviously not rank-1, losing the ability to represent positional relationship. **Bottom:** With aligned block sizes, the factorization is able to recover positional relationship.

3D attention map \mathbf{A} can be represented by Monarch matrices with permutation. We present a more detailed analysis of Monarch parameterizations on attention in Appendix B.3.

3.4 Practical Challenges of MonarchAttention in Video Generation

Aside from the advantages, we identify three challenges that prevent direct usage of MonarchAttention in video generation models.

3.4.1 Challenge 1: Block misalignment with spatiotemporal structure.

The effectiveness of Monarch parameterization critically depends on whether its block structure aligns with the underlying spatiotemporal organization of video tokens. We illustrate this in Figure 7 using a 3D attention example with $(f, h, w) = (2, 3, 3)$, yielding an 18×18 attention matrix, and compare two block configurations.

In the first configuration, we choose block sizes $(b_1, b_2) = (6, 3)$, which group tokens that are spatially adjacent within the same frame, such as $x_{t,i,0}$, $x_{t,i,1}$, and $x_{t,i,2}$. This grouping respects the natural spatiotemporal locality of the video, and as a result, nearly all blocks exhibit an approximately rank-1 structure, leading to a high-quality approximation.

In contrast, choosing block sizes $(9, 2)$ produces blocks of the same total size but groups tokens according to their flattened indices. This grouping mixes tokens that are distant in the original spatiotemporal layout, even though they appear close after flattening. Consequently, most blocks no longer admit a low-rank structure, and the approximation quality degrades sharply. As shown in Figure 1b, aligned block grouping preserves visual fidelity, whereas misaligned grouping leads to severe quality degradation.

This example highlights that, unlike 1D sequences, flattened token order in 3D video does not reflect true spatial or temporal proximity, and that improper block alignment can fundamentally limit the effectiveness of Monarch parameterization.

3.4.2 Challenge 2: Lack of monotonic refinement with increased computation.

Even when block sizes are perfectly aligned with the spatiotemporal structure, semantic interactions may still cause certain blocks to deviate from being rank-1. Crucially, such semantic correspondences are sparse and irregular, making their locations inherently unpredictable. A natural strategy to improve approximation

accuracy is therefore to increase computational budget, e.g., by using smaller blocks that are less likely to mix multiple semantic interactions.

However, in the original Monarch parameterization, increasing computation does not reliably translate into better approximations. Specifically, Monarch enforces the constraint $b_1 b_2 = N$, where $N = fhw$ is the total number of tokens. Under this constraint, the total number of parameters in the Monarch factors scales as $\mathcal{O}(N(b_1 + b_2))$. As a result, changing block sizes (b_1, b_2) redistributes parameters between the two factors \mathbf{L} and \mathbf{R} , but does not guarantee an increase in total computation.

Consequently, the constraint $b_1 b_2 = N$ prevents a monotonic refinement: increasing compute by modifying (b_1, b_2) necessarily trades finer partitioning in one dimension for coarser partitioning in the other, so semantic interactions remain mixed within blocks and the approximation error may not improve.

This contrasts sharply with sparse-attention-based methods (like topk- k), where additional computation directly corresponds to attending to more tokens and thus yields a monotonic accuracy–efficiency trade-off.

3.4.3 Challenge 3: High overhead of iterative refinement.

MonarchAttention estimates the Monarch factors \mathbf{L} and \mathbf{R} through an iterative refinement procedure. While increasing the number of refinement steps generally improves approximation accuracy, it introduces substantial additional computation. Specifically, the runtime of MonarchAttention scales linearly with the number of iterations, directly reducing throughput.

4 MonarchRT

In this section, we propose MONARCHRT by addressing the three challenges identified above, i.e., how to align block sizes effectively (Section 4.1), how to enable finer-grained Monarch parameterization beyond fixed block areas (Section 4.2), and how to reduce the parameterization cost for real-time usage (Section 4.3). We then describe our custom implementation that supports efficient training of MonarchAttention on long sequences.

4.1 Aligning Monarch Blocks

Key insight: A Monarch parameterization is *aligned* with video attention if each spatiotemporal dimension (f, h, w) is entirely contained within exactly one block dimension. Only under this condition can Monarch exactly represent fully separable positional attention patterns.

To formalize this notion, we consider a simplified setting where the attention follows the purely positional model in Equation (1) by temporarily assuming $\mathbf{S} = 0$. Recall that a Monarch matrix is parameterized by two block-diagonal factors \mathbf{L} and \mathbf{R} , which can be interpreted as 3D tensors of shape $b_2 \times b_1 \times b_1$ and $b_1 \times b_2 \times b_2$, respectively, with block sizes b_1 and b_2 satisfying $b_1 b_2 = fhw$.

An aligned construction. Consider choosing block sizes $b_1 = fh$ and $b_2 = w$. In this case, \mathbf{L} has shape $w \times fh \times fh$ and \mathbf{R} has shape $fh \times w \times w$. Under this parameterization, the post-softmax attention scores can be written as

$$\mathbf{A}_{(f_0, h_0, w_0), (f_1, h_1, w_1)} = \mathbf{L}_{w_0, (f_0, h_0), (f_1, h_1)} \mathbf{R}_{(f_1, h_1), w_0, w_1}.$$

By setting

$$\begin{aligned} \mathbf{L}_{w_0, (f_0, h_0), (f_1, h_1)} &= d_t(f_0, f_1) d_h(h_0, h_1), \\ \mathbf{R}_{(f_1, h_1), w_0, w_1} &= d_w(w_0, w_1), \end{aligned}$$

the Monarch parameterization exactly reproduces the fully separable positional attention model in Equation (1). Importantly, any permutation of the dimensions across the block sizes, such as $(b_1, b_2) = (f, hw)$ or $(b_1, b_2) = (fw, h)$, admits an equivalent exact decomposition.

When alignment fails. Crucially, no single dimension (f , h , or w) may be split across both block sizes. If a dimension partially spans b_1 and b_2 , it becomes impossible to factor the attention into fully separable terms \mathbf{L} and \mathbf{R} . As a result, the Monarch approximation cannot exactly represent the assumed attention structure, even with increased parameter count. This explains the behavior observed in Figure 1b, where aligned block sizes (e.g., (fh, w)) preserve visual fidelity, while misaligned choices (e.g., $(f \cdot \frac{h}{4}, 4w)$) lead to severe degradation despite higher nominal capacity.

Take Away

We therefore define a Monarch parameterization for video attention to be *aligned* if each of the video dimensions f , h , and w is fully assigned to exactly one block dimension. Excluding the degenerate dense cases $(fhw, 1)$ and $(1, fhw)$, this yields exactly six aligned block configurations:

$$(fh, w), (w, fh), (f, hw), (hw, f), (fw, h), (h, fw).$$

4.2 Tiled Monarch Parameterization

We begin by recalling the standard Monarch parameterization. Given block sizes (b_1, b_2) with $N = b_1 b_2$, a Monarch matrix $\mathbf{M} \in \mathbb{R}^{N \times N}$ can be written as

$$\mathbf{M}_{mn} = \mathbf{M}_{(\ell b_2 + j)(kb_2 + i)} = \mathbf{L}_{j\ell k} \mathbf{R}_{kji},$$

where $\mathbf{L} \in \mathbb{R}^{b_2 \times b_1 \times b_1}$ and $\mathbf{R} \in \mathbb{R}^{b_1 \times b_2 \times b_2}$.

Algorithm. We propose *Tiled Monarch Parameterization*, which generalizes Monarch by decomposing each Monarch block into smaller sub-blocks. Specifically, we introduce integers c_1 and c_2 such that $c_1 \mid b_1$ and $c_2 \mid b_2$. Instead of a single Monarch factorization, we represent \mathbf{M} as a collection of $c_1^2 c_2^2$ Monarch tiles, each with block sizes $(\frac{b_1}{c_1}, \frac{b_2}{c_2})$.

Formally, we parameterize \mathbf{M} using tiled factors \mathbf{L}' and \mathbf{R}' , where \mathbf{L}' has shape $(c_1, c_2, c_1, c_2, \frac{b_2}{c_2}, \frac{b_1}{c_1}, \frac{b_1}{c_1})$ and \mathbf{R}' has shape $(c_1, c_2, c_1, c_2, \frac{b_1}{c_1}, \frac{b_2}{c_2}, \frac{b_2}{c_2})$. Each tile independently parameterizes a local rank-1 structure.

To estimate tiled Monarch factors for the attention matrix \mathbf{A} , we extend MonarchAttention by applying the same alternating refinement procedure independently to each tile. To enforce row-stochasticity, we impose slightly stronger constraints on the tiled factors, detailed in Section A.2.

Theorem 4.1 (Strict expressiveness of tiled Monarch). *Fix base block sizes (b_1, b_2) with $N = b_1 b_2$, and let $c_1 \mid b_1$, $c_2 \mid b_2$ be tiling factors. Let $\mathcal{M}(b_1, b_2)$ denote the set of Monarch matrices with block sizes (b_1, b_2) , i.e., matrices $\mathbf{M} \in \mathbb{R}^{N \times N}$ that admit factors $\mathbf{L} \in \mathbb{R}^{b_2 \times b_1 \times b_1}$, $\mathbf{R} \in \mathbb{R}^{b_1 \times b_2 \times b_2}$ satisfying*

$$\mathbf{M}_{(\ell b_2 + j)(kb_2 + i)} = \mathbf{L}_{j\ell k} \mathbf{R}_{kji}.$$

Let $\mathcal{M}_{\text{tile}}(b_1, b_2; c_1, c_2)$ denote the set of matrices representable by the tiled Monarch parameterization with the same base block sizes (b_1, b_2) and tiling factors (c_1, c_2) . Then

$$\mathcal{M}(b_1, b_2) \subseteq \mathcal{M}_{\text{tile}}(b_1, b_2; c_1, c_2).$$

Moreover, if $c_1 > 1$ or $c_2 > 1$, the inclusion is strict:

$$\mathcal{M}(b_1, b_2) \subset \mathcal{M}_{\text{tile}}(b_1, b_2; c_1, c_2),$$

i.e., every (untiled) Monarch matrix can be represented exactly by a tiled Monarch matrix with appropriate parameter tying, but there exist tiled Monarch matrices that cannot be represented by any (untiled) Monarch parameterization with block sizes (b_1, b_2) .

In other words, tiled Monarch is strictly more expressive than regular Monarch for the same base block sizes. We formally prove Theorem 4.1 in Appendix B.2. Informally, though, tiled factors increase parameter counts by factors of c_2 and c_1 respectively, for \mathbf{L} and \mathbf{R} . By tying parameters across tiles, one can exactly recover the original Monarch parameterization, so tiled Monarch is intuitively at least as expressive as standard Monarch.

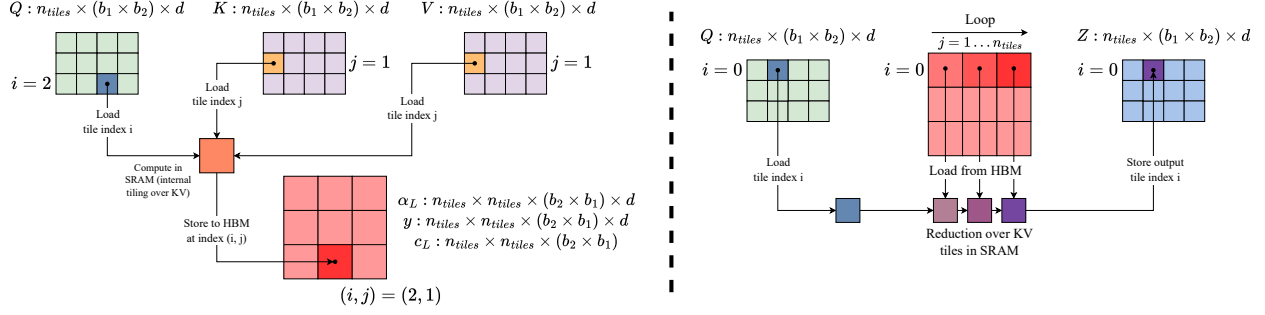


Figure 8 Visualization of efficient kernel implementation for MonarchAttention algorithm with a tiled Monarch parameterization. **Left:** first stage to compute α_L, y, c_L tiles. **Right:** second stage (separate kernel) to compute output by reducing over KV tiles.

Crucially, tiled Monarch enables *controllable refinement*. By increasing (c_1, c_2) , each original block is subdivided into smaller sub-blocks, allowing the approximation to better capture sparse and irregular semantic interactions that cannot be modeled by a single rank-1 block.

Example. Recall that for video attention with resolution (f, h, w) , we set the aligned Monarch block sizes to $(b_1, b_2) = (fh, w)$ as shown in Section 4.1. However, when attention exhibits neighborhood-level sparsity with neighborhood size (n_f, n_h, n_w) , a single Monarch block may span multiple neighborhoods and therefore violate the rank-1 assumption.

Tiled Monarch resolves this issue by enforcing locality within each tile. Specifically, we choose

$$c_1 = \frac{f}{n_f} \cdot \frac{h}{n_h}, \quad c_2 = \frac{w}{n_w},$$

resulting in $c_1 c_2$ Monarch tiles, each with block sizes $(n_f n_h, n_w)$. Each tile therefore contains tokens from only a single spatiotemporal neighborhood along every dimension, making the rank-1 assumption locally valid.

The degenerate case $(n_f, n_h, n_w) = (1, 1, 1)$ reduces to dense attention. Empirically, we find that choosing n_f as a small constant while letting $n_h = \mathcal{O}(h)$ and $n_w = \mathcal{O}(w)$ achieves high visual quality with a sparse parameterization.

Computational complexity. Tiled Monarch preserves the efficient computation pattern of MonarchAttention. Each tile is processed independently using the same alternating refinement procedure, and the overall complexity scales linearly with the number of tiles.

Take Away

In standard Monarch parameterization, changing block shapes does not reliably control either computation cost or expressiveness. In contrast, Tiled Monarch parameterization enables fine-grained block structures and, similar to top- k sparse attention methods, provides a clear and monotonic trade-off between accuracy and efficiency.

4.3 Finetuning and Efficient Implementation

To further reduce the computational overhead of iterative refinement, we introduce *Monarch finetuning*, a lightweight training procedure that dramatically decreases the number of refinement steps required to obtain high-quality Monarch parameterizations. In practice, we find that with finetuning, even a single refinement iteration is often sufficient to match the visual fidelity of much more expensive multi-step optimization.

To enable end-to-end training of Monarch factors, we implement custom forward and backward kernels tailored for long-sequence 3D attention. We visualize the forward process in Figure 8 and provide additional information

Method	Quality Score	Semantic Score	Total Score
Dense Attention	0.844	0.804	0.836
MONARCHRT (95% sparse)	0.846	0.805	0.838

Table 1 VBench scores for base model and trained MONARCHRT on Self-Forcing.

Method	4-step			50-step		
	Quality Score	Semantic Score	Total Score	Quality Score	Semantic Score	Total Score
Dense Attention	0.846	0.800	0.837	0.846	0.810	0.839
VSA (85% sparse)	0.828	0.793	0.821	0.827	0.785	0.819
MONARCHRT (95% sparse)	0.842	0.788	0.832	0.841	0.812	0.835

Table 2 Quality evaluation for a Wan2.1-1.3B (base 50-step and distilled 4-step models) for dense attention as well as trained VSA and MONARCHRT. Higher values indicate better quality for all metrics.

on the MonarchAttention algorithm itself in Sections A.1 and A.2. Similar to the original MonarchAttention, the β terms—and hence the resulting \mathbf{L} and \mathbf{R} factors—can be materialized directly in SRAM using a FlashAttention-style computation pattern. However, the α and \mathbf{c} terms must be materialized in HBM, as their tensor shapes depend jointly on f_q and f_{kv} . For full non-causal 3D attention, this becomes quadratic in the number of frames and would ordinarily be prohibitive.

To overcome this limitation, we adopt a *mini-sequence* strategy: the query frames are divided into smaller chunks, and the complete attention output for each chunk is computed before moving on to the next. This is valid because query frames are independent during the attention computation, allowing us to cap peak memory usage without altering correctness. Since 3D attention workloads are strongly compute-bound, this chunked processing introduces negligible overhead while enabling scalable fintuning of Monarch parameterizations.

5 Empirical Validation

In this section, we demonstrate that MONARCHRT can speed up on top of the SOTA real-time video generation models while preserving video fidelity. We first present MONARCHRT’s generation quality on downstream tasks, then an end-to-end evaluation of MONARCHRT’s throughput.

- In Section 5.1, we demonstrate MONARCHRT preserves generation quality for real-time video generations for Self-Forcing (Huang et al., 2025) with computation cost as little as $\sim 5\%$ of full attention, surpassing existing sparse attention based algorithms.
- in Section 5.2, we conduct further training-free ablations and find again that, even with $\sim 5\%$ attention density, MONARCHRT continues to surpass additional sparse attention baselines, including oracle top- k attention.
- In Section 5.3, we conduct efficiency evaluations and find that our efficient kernel can provide speedups in the range of $1.4 - 11.8\times$ speedups to attention compared to various FlashAttention kernels (Shah et al., 2024). On RTX 5090, we achieve (for the first time) true 16 FPS real-time generation with high quality on Self-Forcing.

5.1 Quality Evaluations

We demonstrate that MONARCHRT can preserve the generation quality in diverse tasks with as low as $\sim 5\%$ attention density.

Setup. We conduct training-free evaluations with VBench (Huang et al., 2023). In order to emphasize the effectiveness of MONARCHRT for auto-regressive and few-step diffusion models, we evaluate MONARCHRT on Self-Forcing (Huang et al., 2025), which is finetuned from Wan 2.1-1.3B (Wan et al., 2025) while applying auto-regressive generation and DMD (Yin et al., 2024b,a) to accommodate real-time generation. We also show

Method	Quality Score	Semantic Score	Total Score
Dense Attention	0.844	0.804	0.836
Exact top- k (85% sparse)	0.834	0.658	0.799
SVG (85% sparse)	0.715	0.214	0.615
RadialAttention (85% sparse)	0.841	0.718	0.816
MONARCHRT (90% sparse)	0.847	0.808	0.839

Table 3 VBench evaluation for Self-Forcing, with all sparse methods evaluated training-free. While SVG and RadialAttention are reported as using an 85% sparse mask, this sparsity level is an overestimate, as the SVG/RadialAttention masks are combined with the autoregressive block-causal mask (and the block-causal mask does not count towards the sparsity level). For RadialAttention and SVG, we also retain the first denoising step (out of 4 for Self-Forcing) and first attention block as dense attention.

Method	4-step				50-step		
	PSNR (↑)	SSIM (↑)	LPIPS (↓)	VBench (↑)	PSNR (↑)	SSIM (↑)	LPIPS (↓)
Dense Attention	—	—	—	0.846	—	—	—
SVG (85% sparse)	9.411	0.203	0.749	0.746	11.349	0.286	0.678
SVG2 (~85% sparse)	11.154	0.321	0.631	0.823	14.625	0.438	0.537
SVG2 (~90% sparse)	10.737	0.307	0.662	0.808	14.116	0.417	0.568
RadialAttention (85% sparse)	11.427	0.290	0.711	0.727	13.719	0.329	0.674
MONARCHRT (90% sparse)	12.657	0.364	0.585	0.834	17.220	0.525	0.506

Table 4 Quality evaluation for a Wan2.1-1.3B (base 50-step and distilled 4-step models). All sparse methods are evaluated training-free. Sparsity levels for SVG2 are average estimates, as the exact sparsity level is not explicitly controllable in SVG2.

results for both Wan 2.1-1.3B (a 50-step bidirectional model) as well as a version of this model that we distilled using DMD to 4 steps.

For Self-Forcing, we inject MONARCHRT directly into the DMD stage of the Self-Forcing training pipeline rather than finetuning on top of the dense Self-Forcing checkpoint. For the 4-step distilled Wan model, we similarly inject MONARCHRT directly into the DMD stage rather than finetuning directly on top of the distilled dense model. For 50-step Wan, we directly apply diffusion loss finetuning on the base model.

Baselines. We mainly evaluate our training-based method against dense baselines as well as VSA (Zhang et al., 2025c), another training-based dynamic sparse attention method, although we do not show VSA results for Self-Forcing as it only supports full bidirectional attention. We compare with additional baselines under a training-free setting in Section 5.2.

Main results and analysis. The results in Table 1 show that MONARCHRT remains close in performance to the dense model for both 1.3B and 14B models, even at 95% effective sparsity. Table Table 2, we observe similar results for bidirectional Wan (both 4-step and 50-step) and find that MONARCHRT outperforms VSA on all metrics, even though it is evaluated at a higher sparsity level.

5.2 Training-Free Ablations

To further demonstrate the effectiveness of Monarch parameterization, we evaluate MONARCHRT against several additional baselines all in a training-free setting.

Setup. We conduct training-free evaluations with VBench (Huang et al., 2023) primarily on Self-Forcing and distilled Wan 2.1-1.3B (4-step).

Baselines. We evaluate the quality of our method against several baselines, including full dense attention and oracle top- k attention. We also include existing SOTA sparse attention methods, namely Sparse VideoGen (Xi et al., 2025), Sparse VideoGen-2 (Yang et al., 2025), and RadialAttention (Li et al., 2025). As these sparse attention methods are only proposed for full bidirectional attention, we mainly compare them with MONARCHRT

for Wan. However, we additionally adapt Sparse VideoGen (SVG) and RadialAttention to Self-Forcing by combining the autoregressive causal mask with their respective static attention masks.

Main results and analysis. As shown in Table 3, SVG fails to produce coherent output by most metrics — notably, the result is produced using SVG with “warmup”, i.e. maintaining dense attention for the first timestep (out of a total 4 steps for Self-Forcing) as well as keeping the first layer as dense attention for all timesteps. The results also show that RadialAttention and oracle top- k both demonstrate notable quality reduction as well relative to the dense baseline, supporting our claim that sparsity is an inherently flawed approximation for video attention. However, training-free MONARCHRT remains quite close to the dense model even with up to 90% sparsity. Similarly, Table 4 shows that MONARCHRT achieves the highest performance over all other sparse methods for the 4-step distilled bidirectional Wan model, both on VBench as well as on other holistic metrics, namely PSNR, SSIM, and LPIPS (Zhang et al., 2018) (we also include these additional metrics on the base 50-step Wan model for reference).

5.3 Efficiency Evaluations

We demonstrate significant speedups for both Self-Forcing and Wan using our efficient Triton kernel implementation. In Tables 5 to 8, we benchmark individual attention kernel latency as well as E2E latency on Nvidia RTX 5090 and H100 GPUs. We compare FA-2 / FA-3 / FA-4 (for RTX 5090 / H100 / B200) to VSA and MONARCHRT at 480p and (theoretical) 720p resolution. We always evaluate MONARCHRT at two sparsity levels, corresponding to block sizes (h, w) and $(3h, w)$ respectively (the latter resulting from $n_f = 3$), where h and w depend on the latent dimensions for the given resolution. For VSA, we measure at 85% sparsity as well as the two effective sparsity levels used for MONARCHRT. Since VSA also requires pre- and post-processing steps, we use `torch.compile` on VSA to provide a fair evaluation.

GPU	Flash Attention	VSA			MONARCHRT	
		$s = 0.85$	$s = 0.95$	$s = 0.97$	$s = 0.95$	$s = 0.97$
RTX 5090	31.15	13.52	8.55	7.89	6.76	3.39
H100	9.74	6.48	4.95	4.60	6.24	2.61
B200	4.53	5.69	4.02	3.65	5.97	2.41

(a) 480p

GPU	Flash Attention	VSA			MONARCHRT	
		$s = 0.85$	$s = 0.97$	$s = 0.98$	$s = 0.97$	$s = 0.98$
RTX 5090	159.11	55.51	24.03	19.84	28.24	13.53
H100	53.29	23.93	13.46	12.15	18.61	9.59
B200	24.78	21.71	11.26	9.86	18.04	9.56

(b) 720p

Table 5 Attention kernel latency (ms) for workload of generating an 81-frame video with Wan 2.1-1.3B. Sparsity level s is indicated for VSA and MONARCHRT.

GPU	Flash Attention	480p		720p		
		MONARCHRT		Flash Attention	MONARCHRT	
		$s = 0.95$	$s = 0.97$		$s = 0.97$	$s = 0.98$
RTX 5090	4.97	1.27	0.63	22.69	4.22	2.01
H100	1.58	1.04	0.57	7.46	2.83	1.53
B200	0.79	0.95	0.45	3.75	2.69	1.49

Table 6 Attention kernel latency (ms) for workload of decoding the final frame in an 81-frame video with Self-Forcing. Sparsity level s is indicated for MONARCHRT.

In Tables 5 and 6, we observe that MONARCHRT achieves up to $9.2\times$ attention speedup over FA-2 on RTX 5090 and up to $3.7\times$ speedup over FA-3 on H100 at 480p resolution. At 720p resolution, these peak speedups become $11.8\times$ and $5.6\times$ respectively. MONARCHRT is also able to achieve theoretical speedups over FA-4, including $\sim 1.4\times$ at 720p for Self-Forcing.

GPU	Flash Attention	VSA			MONARCHRT	
		$s = 0.85$	$s = 0.95$	$s = 0.97$	$s = 0.95$	$s = 0.97$
RTX 5090	7164.56	5244.00	4627.65	4519.46	4866.97	4381.47
H100	2919.98	2723.14	2399.85	2385.24	2530.16	2168.86
(a) 480p						
GPU	Flash Attention	VSA			MONARCHRT	
		$s = 0.85$	$s = 0.97$	$s = 0.98$	$s = 0.97$	$s = 0.98$
RTX 5090	24842.18	15129.24	12661.00	11953.88	12522.81	10626.97
H100	9630.09	6987.10	6209.90	6025.72	6589.27	5706.98
(b) 720p						

Table 7 E2E latency (ms) of generating an 81-frame video with 4-step distilled Wan 2.1-1.3B. Sparsity level s is indicated for VSA and MONARCHRT.

GPU	Flash Attention	480p		720p		
		MONARCHRT		Flash Attention	MONARCHRT	
		$s = 0.95$	$s = 0.97$		$s = 0.97$	$s = 0.98$
RTX 5090	8309.06	6094.45	5697.59	—	—	—
H100	3661.16	3228.45	2962.28	10672.43	7634.64	6815.19

Table 8 E2E latency (ms) of generating an 81-frame video with Self-Forcing. Sparsity level s is indicated for MONARCHRT. 720p results are excluded on RTX 5090 as the KV cache size causes OOM.

This also translates to significant E2E speedups, as shown in Tables 7 and 8. MONARCHRT remains roughly on par with VSA for the same sparsity level. Importantly, MONARCHRT at 95% sparsity outperforms VSA at 85% sparsity both in terms of E2E latency (Table 7) but also in terms of quality (Table 2). Focusing on our 480p Self-Forcing results in Table 8, MONARCHRT at 95% sparsity provides a 36% E2E speedup on RTX 5090 and a 13% E2E speedup on H100.

To provide an additional speedup, we apply `torch.compile` to MONARCHRT and compare it to FA-2 on RTX 5090 for 480p Self-Forcing generation. **Notably, while FA-2 achieves 11 FPS video generation, MonarchRT at 95% sparsity directly achieves 16 FPS** without requiring any additional lossy optimizations such as quantization. 95% sparsity is the same level at which we demonstrate high quality in Section 5.1. To our knowledge, MONARCHRT is one of the first methods to achieve high-quality generation with auto-regressive models in true real-time on consumer-grade hardware.

6 Related Works

Efficient Attention. As transformers have widely grown in adoption across a variety of applications, there has been significant work towards reducing the quadratic cost of softmax attention, both from an algorithmic and from an implementation perspective. FlashAttention (Dao et al., 2022b; Shah et al., 2024) is a fused attention kernel implementation that avoids materializing large attention score matrices in GPU memory and instead computes them on the fly in a tiled manner within on-chip SRAM. For video generation, both static (Zhang

et al., 2025d; Xi et al., 2025; Li et al., 2025) and dynamic (Zhang et al., 2025c; Yang et al., 2025) sparse attention are explored.

7 Conclusion

We have presented MONARCHRT, a principled and efficient attention parameterization for real-time video generation. By analyzing the structure of 3D attention, we showed that its spatiotemporal periodicity and sparse semantic interactions are fundamentally misaligned with existing sparse-attention methods, yet align naturally with the expressive power of Monarch matrices. Building on this insight, our design combines appropriately aligned block structures, the proposed *tiled Monarch parameterization*, and finetuning together with an optimized Triton implementation to deliver substantial speedups while preserving fidelity.

Acknowledgements

We gratefully acknowledge access to NVIDIA computing resources. This work was partially supported by Google Research Award, Google ML & System Junior Faculty Award, Amazon Research Award, Fireworks AI, Intel, Li Auto, Moffett AI, and CMU CyLab Seed funding. This material is also based upon work supported by the National Science Foundation under Grant Nos. CCF-2504353 and CCF-2247014, and by IARPA. Any opinions, findings, conclusions or recommendations expressed are those of the authors and do not necessarily reflect the views of the National Science Foundation.

References

Philip J. Ball, Jakob Bauer, Frank Belletti, Bethanie Brownfield, Ariel Ephrat, Shlomi Fruchter, Agrim Gupta, Kristian Holsheimer, Aleksander Holynski, Jiri Hron, Christos Kaplanis, Marjorie Limont, Matt McGill, Yanko Oliveira, Jack Parker-Holder, Frank Perbet, Guy Scully, Jeremy Shar, Stephen Spencer, Omer Tov, Ruben Villegas, Emma Wang, Jessica Yung, Cip Baetu, Jordi Berbel, David Bridson, Jake Bruce, Gavin Buttimore, Sarah Chakera, Bilva Chandra, Paul Collins, Alex Cullum, Bogdan Damoc, Vibha Dasagi, Maxime Gazeau, Charles Gbadamosi, Woohyun Han, Ed Hirst, Ashyana Kachra, Lucie Kerley, Kristian Kjems, Eva Knoepfel, Vika Koriakin, Jessica Lo, Cong Lu, Zeb Mehring, Alex Moufarek, Henna Nandwani, Valeria Oliveira, Fabio Pardo, Jane Park, Andrew Pierson, Ben Poole, Helen Ran, Tim Salimans, Manuel Sanchez, Igor Saprykin, Amy Shen, Sailesh Sidhwani, Duncan Smith, Joe Stanton, Hamish Tomlinson, Dimple Vijaykumar, Luyu Wang, Piers Wingfield, Nat Wong, Keyang Xu, Christopher Yew, Nick Young, Vadim Zubov, Douglas Eck, Dumitru Erhan, Koray Kavukcuoglu, Demis Hassabis, Zoubin Gharamani, Raia Hadsell, Aäron van den Oord, Inbar Mosseri, Adrian Bolton, Satinder Singh, and Tim Rocktäschel. Genie 3: A new frontier for world models. 2025.

Mathieu Blondel, André F. T. Martins, and Vlad Niculae. Learning classifiers with fenchel-young losses: Generalized entropies, margins, and algorithms, 2019. <https://arxiv.org/abs/1805.09717>.

Beidi Chen, Tri Dao, Eric Winsor, Zhao Song, Atri Rudra, and Christopher Ré. Scatterbrain: Unifying sparse and low-rank attention. *Advances in Neural Information Processing Systems*, 34:17413–17426, 2021.

Özgün Çiçek, Ahmed Abdulkadir, Soeren S. Lienkamp, Thomas Brox, and Olaf Ronneberger. 3d u-net: Learning dense volumetric segmentation from sparse annotation. In Sébastien Ourselin, Leo Joskowicz, Mert R. Sabuncu, Gozde Unal, and William Wells, editors, *Medical Image Computing and Computer-Assisted Intervention – MICCAI 2016*, pages 424–432, Cham, 2016. Springer International Publishing. ISBN 978-3-319-46723-8.

Tri Dao. Flashattention-2: Faster attention with better parallelism and work partitioning. *arXiv preprint arXiv:2307.08691*, 2023.

Tri Dao, Nimit S. Sohoni, Albert Gu, Matthew Eichhorn, Amit Blonder, Megan Leszczynski, Atri Rudra, and Christopher Ré. Kaleidoscope: An efficient, learnable representation for all structured linear maps, 2021. <https://arxiv.org/abs/2012.14966>.

Tri Dao, Beidi Chen, Nimit Sohoni, Arjun Desai, Michael Poli, Jessica Grogan, Alexander Liu, Aniruddh Rao, Atri Rudra, and Christopher Ré. Monarch: Expressive structured matrices for efficient and accurate training, 2022a. <https://arxiv.org/abs/2204.00595>.

Tri Dao, Daniel Y. Fu, Stefano Ermon, Atri Rudra, and Christopher Ré. Flashattention: Fast and memory-efficient exact attention with io-awareness, 2022b. <https://arxiv.org/abs/2205.14135>.

Harry Dong, Xinyu Yang, Zhenyu Zhang, Zhangyang Wang, Yuejie Chi, and Beidi Chen. Get more with less: Synthesizing recurrence with kv cache compression for efficient llm inference. *arXiv preprint arXiv:2402.09398*, 2024.

Dan Fu, Simran Arora, Jessica Grogan, Isys Johnson, Evan Sabri Eryuboglu, Armin Thomas, Benjamin Spector, Michael Poli, Atri Rudra, and Christopher Ré. Monarch mixer: A simple sub-quadratic gemm-based architecture. *Advances in Neural Information Processing Systems*, 36:77546–77603, 2023.

Mutian He and Philip N. Garner. Alleviating forgetfulness of linear attention by hybrid sparse attention and contextualized learnable token eviction, 2025. <https://arxiv.org/abs/2510.20787>.

Xun Huang, Zhengqi Li, Guande He, Mingyuan Zhou, and Eli Shechtman. Self forcing: Bridging the train-test gap in autoregressive video diffusion, 2025. <https://arxiv.org/abs/2506.08009>.

Ziqi Huang, Yinan He, Jiashuo Yu, Fan Zhang, Chenyang Si, Yuming Jiang, Yuanhan Zhang, Tianxing Wu, Qingyang Jin, Nattapol Chanpaisit, Yaohui Wang, Xinyuan Chen, Limin Wang, Dahua Lin, Yu Qiao, and Ziwei Liu. Vbench: Comprehensive benchmark suite for video generative models, 2023. <https://arxiv.org/abs/2311.17982>.

Xingyang Li, Muyang Li, Tianle Cai, Haocheng Xi, Shuo Yang, Yujun Lin, Lvmin Zhang, Songlin Yang, Jinbo Hu, Kelly Peng, Maneesh Agrawala, Ion Stoica, Kurt Keutzer, and Song Han. Radial attention: $o(n \log n)$ sparse attention with energy decay for long video generation, 2025. <https://arxiv.org/abs/2506.19852>.

Enshu Liu, Xuefei Ning, Yu Wang, and Zinan Lin. Distilled decoding 1: One-step sampling of image auto-regressive models with flow matching. *arXiv preprint arXiv:2412.17153*, 2024.

Enshu Liu, Qian Chen, Xuefei Ning, Shengen Yan, Guohao Dai, Zinan Lin, and Yu Wang. Distilled decoding 2: One-step sampling of image auto-regressive models with conditional score distillation. *arXiv preprint arXiv:2510.21003*, 2025.

Adam Polyak, Amit Zohar, Andrew Brown, Andros Tjandra, Animesh Sinha, Ann Lee, Apoorv Vyas, Bowen Shi, Chih-Yao Ma, Ching-Yao Chuang, et al. Movie gen: A cast of media foundation models. *arXiv preprint arXiv:2410.13720*, 2024.

Olaf Ronneberger, Philipp Fischer, and Thomas Brox. U-net: Convolutional networks for biomedical image segmentation, 2015. <https://arxiv.org/abs/1505.04597>.

Christopher De Sa, Albert Gu, Rohan Puttagunta, Christopher Ré, and Atri Rudra. A two pronged progress in structured dense matrix multiplication, 2017. <https://arxiv.org/abs/1611.01569>.

Jay Shah, Ganesh Bikshandi, Ying Zhang, Vijay Thakkar, Pradeep Ramani, and Tri Dao. Flashattention-3: Fast and accurate attention with asynchrony and low-precision, 2024. <https://arxiv.org/abs/2407.08608>.

Wenqiang Sun, Haiyu Zhang, Haoyuan Wang, Junta Wu, Zehan Wang, Zhenwei Wang, Yunhong Wang, Jun Zhang, Tengfei Wang, and Chunchao Guo. Worldplay: Towards long-term geometric consistency for real-time interactive world modeling, 2025. <https://arxiv.org/abs/2512.14614>.

Robbyant Team, Zelin Gao, Qiuyu Wang, Yanhong Zeng, Jiapeng Zhu, Ka Leong Cheng, Yixuan Li, Hanlin Wang, Yinghao Xu, Shuailei Ma, Yihang Chen, Jie Liu, Yansong Cheng, Yao Yao, Jiayi Zhu, Yihao Meng, Kecheng Zheng, Qingyan Bai, Jingye Chen, Zehong Shen, Yue Yu, Xing Zhu, Yujun Shen, and Hao Ouyang. Advancing open-source world models, 2026. <https://arxiv.org/abs/2601.20540>.

Hansi Teng, Hongyu Jia, Lei Sun, Lingzhi Li, Maolin Li, Mingqiu Tang, Shuai Han, Tianning Zhang, WQ Zhang, Weifeng Luo, et al. Magi-1: Autoregressive video generation at scale. *arXiv preprint arXiv:2505.13211*, 2025.

Team Wan, Ang Wang, Baole Ai, Bin Wen, Chaojie Mao, Chen-Wei Xie, Di Chen, Feiwu Yu, Haiming Zhao, Jianxiao Yang, Jianyuan Zeng, Jiayu Wang, Jingfeng Zhang, Jingren Zhou, Jinkai Wang, Jixuan Chen, Kai Zhu, Kang Zhao, Keyu Yan, Lianghua Huang, Mengyang Feng, Ningyi Zhang, Pandeng Li, Pingyu Wu, Ruihang Chu, Ruili Feng, Shiwei Zhang, Siyang Sun, Tao Fang, Tianxing Wang, Tianyi Gui, Tingyu Weng, Tong Shen, Wei Lin, Wei Wang, Wei Wang, Wenmeng Zhou, Wente Wang, Wenting Shen, Wenyuan Yu, Xianzhong Shi, Xiaoming Huang, Xin Xu, Yan Kou, Yangyu Lv, Yifei Li, Yijing Liu, Yiming Wang, Yingya Zhang, Yitong Huang, Yong Li, You Wu, Yu Liu, Yulin Pan, Yun Zheng, Yuntao Hong, Yupeng Shi, Yutong Feng, Zeyinzi Jiang, Zhen Han, Zhi-Fan Wu, and Ziyu Liu. Wan: Open and advanced large-scale video generative models, 2025. <https://arxiv.org/abs/2503.20314>.

Haocheng Xi, Shuo Yang, Yilong Zhao, Chenfeng Xu, Muyang Li, Xiuyu Li, Yujun Lin, Han Cai, Jintao Zhang, Dacheng Li, Jianfei Chen, Ion Stoica, Kurt Keutzer, and Song Han. Sparse videogen: Accelerating video diffusion transformers with spatial-temporal sparsity, 2025. <https://arxiv.org/abs/2502.01776>.

Shuo Yang, Haocheng Xi, Yilong Zhao, Muyang Li, Jintao Zhang, Han Cai, Yujun Lin, Xiuyu Li, Chenfeng Xu, Kelly Peng, et al. Sparse videogen2: Accelerate video generation with sparse attention via semantic-aware permutation. *arXiv preprint arXiv:2505.18875*, 2025.

Can Yaras, Alec S. Xu, Pierre Abillama, Changwoo Lee, and Laura Balzano. Monarchattention: Zero-shot conversion to fast, hardware-aware structured attention, 2025. <https://arxiv.org/abs/2505.18698>.

Tianwei Yin, Michaël Gharbi, Taesung Park, Richard Zhang, Eli Shechtman, Fredo Durand, and William T. Freeman. Improved distribution matching distillation for fast image synthesis, 2024a. <https://arxiv.org/abs/2405.14867>.

Tianwei Yin, Michaël Gharbi, Richard Zhang, Eli Shechtman, Fredo Durand, William T. Freeman, and Taesung Park. One-step diffusion with distribution matching distillation, 2024b. <https://arxiv.org/abs/2311.18828>.

Tianwei Yin, Qiang Zhang, Richard Zhang, William T Freeman, Fredo Durand, Eli Shechtman, and Xun Huang. From slow bidirectional to fast autoregressive video diffusion models. In *Proceedings of the Computer Vision and Pattern Recognition Conference*, pages 22963–22974, 2025.

Jintao Zhang, Haoxu Wang, Kai Jiang, Shuo Yang, Kaiwen Zheng, Haocheng Xi, Ziteng Wang, Hongzhou Zhu, Min Zhao, Ion Stoica, Joseph E. Gonzalez, Jun Zhu, and Jianfei Chen. Sla: Beyond sparsity in diffusion transformers via fine-tunable sparse-linear attention, 2025a. <https://arxiv.org/abs/2509.24006>.

Jintao Zhang, Kaiwen Zheng, Kai Jiang, Haoxu Wang, Ion Stoica, Joseph E Gonzalez, Jianfei Chen, and Jun Zhu. Turbodiffusion: Accelerating video diffusion models by 100-200 times. *arXiv preprint arXiv:2512.16093*, 2025b.

Peiyuan Zhang, Yongqi Chen, Haofeng Huang, Will Lin, Zhengzhong Liu, Ion Stoica, Eric Xing, and Hao Zhang. Vsa: Faster video diffusion with trainable sparse attention, 2025c. <https://arxiv.org/abs/2505.13389>.

Peiyuan Zhang, Yongqi Chen, Runlong Su, Hangliang Ding, Ion Stoica, Zhengzhong Liu, and Hao Zhang. Fast video generation with sliding tile attention, 2025d. <https://arxiv.org/abs/2502.04507>.

Richard Zhang, Phillip Isola, Alexei A. Efros, Eli Shechtman, and Oliver Wang. The unreasonable effectiveness of deep features as a perceptual metric, 2018. <https://arxiv.org/abs/1801.03924>.

Yang Zhou, Hongyi Liu, Zhuoming Chen, Yuandong Tian, and Beidi Chen. Gsm-infinite: How do your llms behave over infinitely increasing context length and reasoning complexity?, 2025. <https://arxiv.org/abs/2502.05252>.

Appendix

A MonarchAttention Algorithm

A.1 Original MonarchAttention

Algorithm 1. Below are the updates that MonarchAttention uses in a single iteration, derived from optimizing the objective function with respect to \mathbf{L} and \mathbf{R} individually:

$$\begin{aligned}\boldsymbol{\alpha}_{R,kjv}^{(t)} &= \sum_{\ell} \mathbf{L}_{j\ell k}^{(t-1)} \mathbf{Q}_{\ell jv}, \quad \mathbf{c}_{R,kj}^{(t)} = \sum_{\ell} \mathbf{L}_{j\ell k}^{(t-1)} \\ \boldsymbol{\beta}_{R,kji}^{(t)} &= \sum_v \boldsymbol{\alpha}_{R,kjv}^{(t)} \mathbf{K}_{kiv} \\ \mathbf{R}^{(t)} &= \text{softmax}_i \left(\mathbf{Z}_R^{(t)} \right), \quad \mathbf{Z}_{R,kji}^{(t)} = \boldsymbol{\beta}_{R,kji}^{(t)} / \mathbf{c}_{R,kj}^{(t)} \\ \boldsymbol{\alpha}_{L,jkv}^{(t)} &= \sum_i \mathbf{R}_{kji}^{(t)} \mathbf{K}_{kiv}, \quad \mathbf{c}_{L,jk}^{(t)} = \sum_l \mathbf{R}_{kji}^{(t)} \log \mathbf{R}_{kji}^{(t)} \\ \boldsymbol{\beta}_{L,j\ell k}^{(t)} &= \sum_v \boldsymbol{\alpha}_{L,j\ell k}^{(t)} \mathbf{Q}_{\ell jv} \\ \mathbf{L}^{(t)} &= \text{softmax}_k \left(\mathbf{Z}_L^{(t)} \right), \quad \mathbf{Z}_{L,j\ell k}^{(t)} = \boldsymbol{\beta}_{L,j\ell k}^{(t)} - \mathbf{c}_{L,jk}^{(t)}\end{aligned}$$

where we interpret \mathbf{Q} and \mathbf{K} as $b_1 \times b_2 \times d$ tensors. Then, to obtain the output via \mathbf{V} ,

$$\mathbf{Y}_{kju} = \sum_i \mathbf{R}_{kji} \mathbf{V}_{kiv}, \quad \mathbf{O}_{\ell ju} = \sum_k \mathbf{L}_{j\ell k} \mathbf{Y}_{kju}$$

where we also interpret \mathbf{V} as a $b_1 \times b_2 \times d$ tensor. We have also provided pseudocode for the MonarchAttention algorithm in Figure 9a.

A.2 Modified MonarchAttention using Tiled Monarch Parameterization

Under our tiled Monarch parameterization, we adopt the following set of updates for iteratively refining \mathbf{L} and \mathbf{R} , which are also derived from optimizing the objective function with respect to \mathbf{L} and \mathbf{R} individually:

$$\begin{aligned}\boldsymbol{\alpha}_{R,\ell_1 j_1 k_1 i_1 k_2 j_2 v}^{(t)} &= \sum_{\ell_2} \mathbf{L}_{\ell_1 j_1 k_1 i_1 j_2 \ell_2 k_2}^{(t-1)} \mathbf{Q}_{\ell_1 \ell_2 j_1 j_2 v} \\ \mathbf{c}_{R,\ell_1 j_1 k_1 i_1 k_2 j_2}^{(t)} &= \sum_{\ell_2} \mathbf{L}_{\ell_1 j_1 k_1 i_1 j_2 \ell_2 k_2}^{(t-1)} \\ \boldsymbol{\beta}_{R,\ell_1 j_1 k_1 i_1 k_2 j_2 i_2}^{(t)} &= \sum_v \boldsymbol{\alpha}_{R,\ell_1 j_1 k_1 i_1 k_2 j_2 v}^{(t)} \mathbf{K}_{k_1 k_2 i_1 i_2 v} \\ \mathbf{R}^{(t)} &= \text{softmax}_{i_2} \left(\mathbf{Z}_R^{(t)} \right), \\ \mathbf{Z}_{R,\ell_1 j_1 k_1 i_1 k_2 j_2 i_2}^{(t)} &= \boldsymbol{\beta}_{R,\ell_1 j_1 k_1 i_1 k_2 j_2 i_2}^{(t)} / \mathbf{c}_{R,\ell_1 j_1 k_1 i_1 k_2 j_2}^{(t)} \\ \boldsymbol{\alpha}_{L,\ell_1 j_1 k_1 i_1 j_2 k_2 v}^{(t)} &= \sum_{i_2} \mathbf{R}_{\ell_1 j_1 k_1 i_1 k_2 j_2 i_2}^{(t)} \mathbf{K}_{k_1 k_2 i_1 i_2 v} \\ \mathbf{c}_{L,\ell_1 j_1 k_1 i_1 j_2 k_2}^{(t)} &= \sum_{i_2} \mathbf{R}_{\ell_1 j_1 k_1 i_1 k_2 j_2 i_2}^{(t)} \log \mathbf{R}_{\ell_1 j_1 k_1 i_1 k_2 j_2 i_2}^{(t)} \\ \boldsymbol{\beta}_{L,\ell_1 j_1 k_1 i_1 j_2 \ell_2 k_2}^{(t)} &= \sum_v \boldsymbol{\alpha}_{L,\ell_1 j_1 k_1 i_1 j_2 k_2 v}^{(t)} \mathbf{Q}_{\ell_1 \ell_2 j_1 j_2 v} \\ \mathbf{L}^{(t)} &= \text{softmax}_{k_1, k_2, i_1} \left(\mathbf{Z}_L^{(t)} \right), \\ \mathbf{Z}_{L,\ell_1 j_1 k_1 i_1 j_2 \ell_2 k_2}^{(t)} &= \boldsymbol{\beta}_{L,\ell_1 j_1 k_1 i_1 j_2 \ell_2 k_2}^{(t)} - \mathbf{c}_{L,\ell_1 j_1 k_1 i_1 j_2 k_2}^{(t)}\end{aligned}$$

where we interpret \mathbf{Q} and \mathbf{K} as $c_1 \times \frac{b_1}{c_1} \times c_2 \times \frac{b_2}{c_2} \times d$ tensors. Then to obtain the final attention output via \mathbf{V} :

$$\mathbf{Y}_{\ell_1 j_1 k_1 i_1 j_2 k_2 v} = \sum_{i_2} \mathbf{R}_{\ell_1 j_1 k_1 i_1 k_2 j_2 i_2} \mathbf{V}_{k_1 k_2 i_1 i_2 v}$$

$$\mathbf{O}_{\ell_1 \ell_2 j_1 j_2 v} = \sum_{k_1, k_2, i_1} \mathbf{L}_{\ell_1 j_1 k_1 i_1 j_2 \ell_2 k_2} \mathbf{Y}_{\ell_1 j_1 k_1 i_1 j_2 k_2 v}$$

As these update rules may be difficult to interpret, we have provided pseudocode for this algorithm in Figure 9b. In our efficient Triton kernel implementation, we adopt the same approach as MonarchAttention to avoid materializing \mathbf{L} and \mathbf{R} in HBM and instead use a FlashAttention-like implementation that computes them on-the-fly in SRAM.

```

# Q: array of size (N, d)
# K: array of size (N, d)
# V: array of size (N, d)
# T: number of steps
# b1, b2: block sizes

def monarch_attention(Q, K, V, T, b1, b2):
    L = stack(b2 * [eye(b1)])
    Q = Q.view(b1, b2, d)
    K = K.view(b1, b2, d)

    for t in range(T):
        aR = einsum("jkl,ljv->kjv", L, Q)
        bR = einsum("kjkv,kiv->kji", aR, K)
        cR = einsum("jkl->kj", L)
        R = softmax(bR / cR[:, :, None], axis=2)

        aL = einsum("kji,kiv->jkv", R, K)
        bL = einsum("jkv,ljv->jkl", aL, Q)
        cL = einsum("kji->jk", R * log(R))
        L = softmax(bL - cL[:, :, None], axis=1)

        V = V.view(b1, b2, d)
        Y = einsum("kji,kiv->jkv", R, V)
        Z = einsum("jkl,jkv->ljv", L, Y)
        O = Z.view(N, d)

    return O

```

```

# Q: array of size (N, d)
# K: array of size (N, d)
# V: array of size (N, d)
# T: number of steps
# bb1, bb2: base block sizes
# c1, c2: tiling factors

def tiled_monarch_attention(Q, K, V, T,
                            bb1, bb2, c1, c2):
    ntiles = c1 * c2
    b1 = bb1 // c1
    b2 = bb2 // c2
    L = stack(ntiles * [stack(ntiles * [
        stack(b2 * [eye(b1)])
    ])])
    Q = rearrange(Q, "(albj)v -> (ab)ljv",
                  a=c1, b=c2, l=b1, j=b2)
    Q = rearrange(K, "(akbi)v -> (ab)kiv",
                  a=c1, b=c2, k=b1, i=b2)

    for t in range(T):
        aR = einsum("mnjkl,mljv->mnkjv", L, Q)
        bR = einsum("mnkjv,nkiv->mnkji", aR, K)
        cR = einsum("mnjkl->mnkj", L)
        R = softmax(bR / cR[:, :, :, :, None], axis=4)

        aL = einsum("mnkji,nkiv->mnjkv", R, K)
        bL = einsum("mnjkv,mljv->mnjkl", aL, Q)
        cL = einsum("mnkji->mnjk", R * log(R))
        L = softmax(bL - cL[:, :, :, :, None], axis=(1, 3))

        V = rearrange(V, "(akbi)v -> (ab)kiv",
                      a=c1, b=c2, k=b1, i=b2)
        Y = einsum("mnkji,nkiv->mnjkv", R, V)
        Z = einsum("mnjkl,mnjkv->mljv", L, Y)
        O = rearrange(Z, "(ab)ljv -> (albj)v",
                      a=c1, b=c2, l=b1, j=b2)

    return O

```

(a) MonarchAttention pseudocode

(b) Tiled MonarchAttention pseudocode

Figure 9 Pseudocode for MonarchAttention variants. (a) Standard pseudocode for MonarchAttention, based directly off of the pseudocode provided by Yaras et al. (2025). (b) Modified pseudocode for MonarchAttention to support tiled Monarch parameterization.

B Proofs and Analysis

B.1 Proof for Theorem 3.1

Let f, h, w denote the number of frames, height, and width respectively, so the total number of tokens is $N = fhw$ and the attention matrix $A \in \mathbb{R}^{N \times N}$ is indexed by pairs of spatiotemporal positions

$$p = (f_0, h_0, w_0), q = (f_1, h_1, w_1).$$

Assume a row-major ordering of tokens along the time, height, and width dimensions. Under the attention map model in Equation (1), each entry of A decomposes as

$$A_{pq} = D_{pq} + S_{pq} + \epsilon,$$

where the positional term factorizes along the three axes as

$$D_{pq} = d_w(w_0, w_1) d_h(h_0, h_1) d_t(f_0, f_1).$$

We show that D can be written as a row-wise permutation of a blockwise rank-1 matrix with D' (using permutation P).

Assume a standard row-major token ordering on the frame, height, and width indices, the width dimension being contiguous in the flattened token sequence. Concretely, the absolute index $\phi(f_0, h_0, w_0)$ of a token with spatiotemporal indices (f_0, h_0, w_0) is

$$\phi(f_0, h_0, w_0) = ((f_0 h) + h_0) w + w_0.$$

We can also consider a permuted token ordering that makes width noncontiguous:

$$\rho(f_0, h_0, w_0) = w_0 f h + (f_0 h + h_0).$$

Let $P \in \mathbb{R}^{N \times N}$ be the permutation matrix that maps the token ordering $\rho \rightarrow \phi$, i.e.

$$P_{\phi(f_0, h_0, w_0), \rho(f_0, h_0, w_0)} = 1$$

and zero elsewhere. Then define

$$D' = P^\top D,$$

so that D' is obtained from D by a row-wise permutation that maps the original row-major indices from ϕ to column-major indices given by ρ . Importantly,

$$D = P D'$$

We now prove that D' is blockwise rank-1. Using block sizes $(b_1, b_2) = (fh, w)$, we take a 4D blocked view of D' with shape (b_2, b_1, b_1, b_2) , so $D'_{j,:,:,:}$ is a block of size $b_1 \times b_2$ for all $j \in [b_2], k \in [b_1]$. Due to the row-wise permutation, the rows of D' (corresponding to query tokens) follow the column-major ordering while the columns (corresponding to key tokens) follow the row-major ordering. For convenience, let us define

$$\sigma(f_0, h_0) = f_0 h + h_0$$

to map the frame and height indices for a given token to a combined (row-major) time/height index so that $\sigma(f_0, h_0) \in [b_1]$. Then we can also define $d_{t,h}$:

$$d_{t,h}(\sigma(f_0, h_0), \sigma(f_1, h_1)) = d_t(f_0, f_1) d_h(h_0, h_1)$$

which takes combined time/height indices for two tokens and computes the combined time-wise and height-wise components of the positional attention score for the two tokens.

Let $B^{(j,k)} = D'_{j,:,:,:} \in \mathbb{R}^{b_1 \times b_2}$ denote the (j, k) -th block of D' . Note that columns of $B^{(j,k)}$ correspond to the key/value tokens with the same time/height index while rows of $B^{(j,k)}$, due to the row-wise permutation for D' , correspond to query tokens with the same width index. This means

$$B_{i,l}^{(j,k)} = d_w(j, l) d_{t,h}(i, k)$$

Alternatively,

$$\mathbf{B}^{(j,k)} = \begin{bmatrix} d_{t,h}(0,k) \\ d_{t,h}(1,k) \\ \vdots \\ d_{t,h}(b_1-1,k) \end{bmatrix} \begin{bmatrix} d_w(j,0) \\ d_w(j,1) \\ \vdots \\ d_w(j,b_2-1) \end{bmatrix}^\top$$

So $\mathbf{B}^{(j,k)}$ is rank-1, meaning \mathbf{D}' is blockwise rank-1.

Therefore, since Equation (1) defines

$$\mathbf{A} = \mathbf{D} + \mathbf{S} + \epsilon$$

and since

$$\mathbf{D} = \mathbf{P}\mathbf{D}'$$

then

$$\mathbf{A} = \mathbf{P}\mathbf{D}' + \mathbf{S} + \epsilon$$

where \mathbf{P} is a permutation matrix, \mathbf{D}' is blockwise rank-1 with block sizes (b_1, b_2) that satisfy $b_1 b_2 = fhw$, and \mathbf{S} is a sparse matrix.

Note that the proof can be generalized for any of the “proper” block sizes specified in Section 4.1, so long as the appropriate sequence flattening order and permutation (defined by ϕ and ρ) are used.

B.2 Proof for Theorem 4.1

(Containment). Let $\mathbf{M} \in \mathcal{M}(b_1, b_2)$ with factors (\mathbf{L}, \mathbf{R}) . Let $c_1 \mid b_1, c_2 \mid b_2$ be tiling factors, and write $\tilde{b}_1 := b_1/c_1, \tilde{b}_2 := b_2/c_2$. Now define tiled factors $(\mathbf{L}', \mathbf{R}')$ by parameter tying: for all valid indices,

$$\mathbf{L}'_{\ell_1, j_1, k_1, i_1, j_2, \ell_2, k_2} := \mathbf{L}_{j, \ell, k} \quad \text{with} \quad j = j_1 \tilde{b}_2 + j_2, \ell = \ell_1 \tilde{b}_1 + \ell_2, k = k_1 \tilde{b}_1 + k_2,$$

i.e., \mathbf{L}' ignores i_1 , and

$$\mathbf{R}'_{\ell_1, j_1, k_1, i_1, k_2, j_2, i_2} := \mathbf{R}_{k, j, i} \quad \text{with} \quad i = i_1 \tilde{b}_2 + i_2, j = j_1 \tilde{b}_2 + j_2, k = k_1 \tilde{b}_1 + k_2,$$

i.e., \mathbf{R}' ignores ℓ_1 . Substituting these definitions into the tiled formula yields

$$\mathbf{L}'_{\ell_1, j_1, k_1, i_1, j_2, \ell_2, k_2} \mathbf{R}'_{\ell_1, j_1, k_1, i_1, k_2, j_2, i_2} = \mathbf{L}_{j, \ell, k} \mathbf{R}_{k, j, i} = \mathbf{M}_{(\ell b_2 + j)(k b_2 + i)},$$

so $\mathbf{M} \in \mathcal{M}_{\text{tile}}(b_1, b_2; c_1, c_2)$. Hence $\mathcal{M}(b_1, b_2) \subseteq \mathcal{M}_{\text{tile}}(b_1, b_2; c_1, c_2)$.

(Strictness). Assume $c_1 > 1$ or $c_2 > 1$, so at least one of $\tilde{b}_1 < b_1$ or $\tilde{b}_2 < b_2$ holds, meaning that a slice $\mathbf{B}^{(j,k)} \in \mathbb{R}^{b_1 \times b_2}$ can contain *multiple* rank-1 tiles. We construct a tiled matrix whose $(j, k) = (0, 0)$ slice has rank 2, which is impossible to represent exactly for untiled Monarch.

Consider the slice $\mathbf{B}^{(0,0)}$ (fix $j = 0, k = 0$). Pick two distinct rows $r_1 \neq r_2$ and two distinct columns $s_1 \neq s_2$ such that (r_1, s_1) and (r_2, s_2) lie in *different tiles* of the $c_1 \times c_2$ tiling of $\{0, \dots, b_1-1\} \times \{0, \dots, b_2-1\}$. (This is always possible when $c_1 > 1$ or $c_2 > 1$: if $c_1 > 1$, choose r_1 and r_2 from different row-tiles; if $c_2 > 1$, choose s_1 and s_2 from different column-tiles.)

Define a tiled Monarch matrix \mathbf{M} by setting all tiles to zero except the two tiles containing (r_1, s_1) and (r_2, s_2) , and within each of these two tiles choose local factors so that the tile equals a single-entry rank-1 matrix with value 1 at that coordinate (and zeros elsewhere). This is feasible because each tile independently parameterizes an arbitrary rank-1 matrix on its $\tilde{b}_1 \times \tilde{b}_2$ support.

Then $\mathbf{B}^{(0,0)}$ has exactly two nonzero entries: $\mathbf{B}_{r_1, s_1}^{(0,0)} = 1$ and $\mathbf{B}_{r_2, s_2}^{(0,0)} = 1$. The 2×2 submatrix of $\mathbf{B}^{(0,0)}$ restricted to rows $\{r_1, r_2\}$ and columns $\{s_1, s_2\}$ is the identity matrix, hence $\text{rank}(\mathbf{B}^{(0,0)}) \geq 2$. Therefore $\mathbf{M} \notin \mathcal{M}(b_1, b_2)$, since every (j, k) slice of an untiled Monarch matrix must have rank at most 1. But by construction $\mathbf{M} \in \mathcal{M}_{\text{tile}}(b_1, b_2; c_1, c_2)$. Thus the containment is strict whenever $c_1 > 1$ or $c_2 > 1$.

B.3 Attention Maps as Monarch Matrices

In this section, we formalize the notion from Section 3.3 that the attention map, which admits rank-1 blocks based on our case-by-case analysis, can be represented as a Monarch matrix via permutation. We use the same blocked indexing and notation as in Section 3.3.

By assumption, the permuted attention matrix $\tilde{\mathbf{A}} \in \mathbb{R}^{N \times N}$ is partitioned into blocks $\tilde{\mathbf{A}}_{[j,k]} \in \mathbb{R}^{b_1 \times b_2}$, with $j \in [b_2], k \in [b_1]$ and $b_1 b_2 = N$, and each block is rank-1. Thus, for every (j, k) there exist vectors $\mathbf{u}^{(j,k)} \in \mathbb{R}^{b_1}$ and $\mathbf{v}^{(j,k)} \in \mathbb{R}^{b_2}$ such that

$$\tilde{\mathbf{A}}_{[j,k]} = \mathbf{u}^{(j,k)} (\mathbf{v}^{(j,k)})^\top, \quad \text{i.e.} \quad \tilde{\mathbf{A}}_{[j,k]}(\ell, i) = \mathbf{u}_\ell^{(j,k)} \mathbf{v}_i^{(j,k)}$$

We now construct the Monarch factors directly from these blockwise rank-1 decompositions. Define

$$\mathbf{L}_{j\ell k} = \mathbf{u}_\ell^{(j,k)}, \quad \mathbf{R}_{kji} = \mathbf{v}_i^{(j,k)}$$

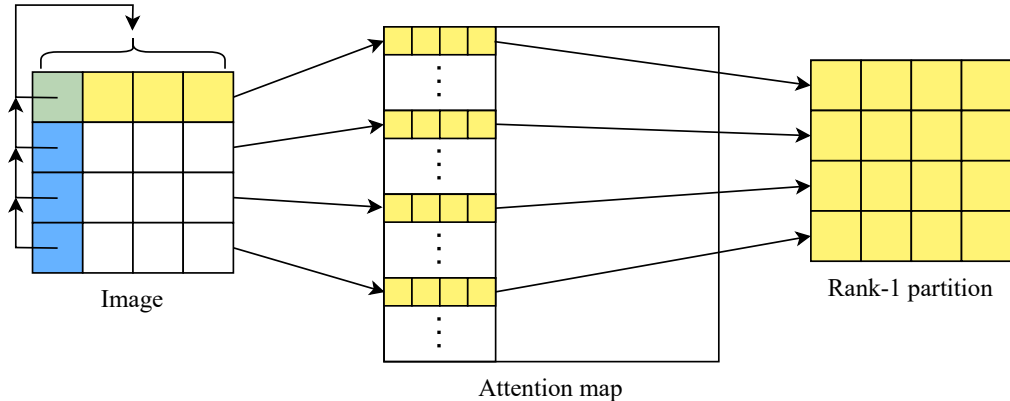
Then, under the same blocked indexing used for Monarch matrices in Section 2, we have

$$\tilde{\mathbf{A}}_{[j,k]}(\ell, i) = \mathbf{L}_{j\ell k} \mathbf{R}_{kji}$$

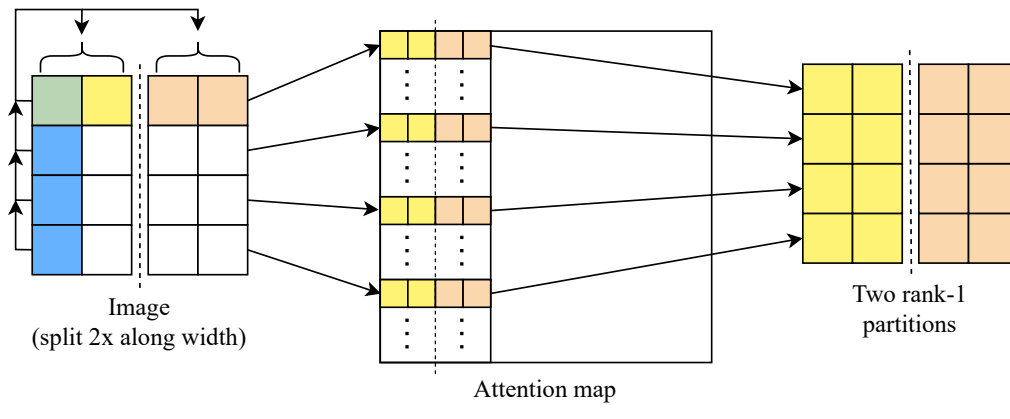
Since $\mathbf{A} = \mathbf{P} \tilde{\mathbf{A}}$, then we also have

$$\mathbf{A}_{ljk} = \mathbf{L}_{j\ell k} \mathbf{R}_{kji}$$

when we take the 4D view of \mathbf{A} . This matches the Monarch parameterization exactly. Therefore $\mathbf{A} = \mathbf{P} \tilde{\mathbf{A}}$ is a Monarch matrix with block sizes (b_1, b_2) when $\tilde{\mathbf{A}}$ is blockwise rank-1.



(a) Untiled (h, w) block size partitioning



(b) Tiled $(h, \frac{w}{2})$

Figure 10 Illustration of untiled/tiled block size partitioning schemes.

B.4 Block Size Analysis

For simplicity, let us consider the single image case ($f = 1$). Based on the block size analysis conducted in Section 4.1, block sizes (h, w) would enable a proper Monarch parameterization of the positional component of the $hw \times hw$ attention map. With these block sizes, the parameterization effectively forms partitions of the attention map that contain pairwise attention scores between all tokens in a given column and all tokens in a given row of the image. This allows each partition to be rank-1 (under the assumptions from Equation (1)), enabling a proper parameterization. We illustrate this blocking scheme in Figure 10a. Using different block sizes (e.g. $(2h, \frac{w}{2})$) would cause each partition to span all tokens along multiple columns or multiple rows of the image, which would remove the rank-1 structure as previously noted. Importantly, this restricts block sizes to be equivalent to the video dimensions.

In Section 4.2, we introduce a tiled Monarch parameterization to reduce this constraint. Effectively, our modified parameterization to an extent enables decoupling the block size selection from the actual video dimensions. We illustrate how this parameterization functions in Figure 10b in the case where we select one of the block sizes as $\frac{w}{2}$. In the tiled parameterization, by applying the appropriate permutation/blocking, we gain much more flexibility in how we select our block sizes, which decide how rank-1 partitions are formed.

C Extended Results

We provide the extended VBench results corresponding to our previous evaluations in Sections 5.1 and 5.2. The extended results generally corroborate the conclusions we drew from our overall empirical evaluations.

C.1 Extended Trained Results

Metric	Dense Attention	MONARCHRT (95% sparse)
Subject Consistency	0.959	0.954
Background Consistency	0.960	0.956
Temporal Flickering	0.990	0.991
Motion Smoothness	0.985	0.984
Dynamic Degree	0.653	0.747
Aesthetic Quality	0.650	0.640
Imaging Quality	0.680	0.672
Object Class	0.946	0.949
Multiple Objects	0.859	0.855
Human Action	0.966	0.968
Color	0.872	0.884
Spatial Relationship	0.776	0.776
Scene	0.580	0.575
Appearance Style	0.205	0.202
Temporal Style	0.244	0.245
Overall Consistency	0.265	0.266
Quality Score	0.844	0.846
Semantic Score	0.804	0.805
Total Score	0.836	0.838

Table 9 Extended VBench scores from Table 1 for base model and trained MONARCHRT on Self-Forcing.

Metric	4-step			50-step		
	Dense Attention	VSA (90% sparse)	MONARCHRT (95% sparse)	Dense Attention	VSA (90% sparse)	MONARCHRT (95% sparse)
Subject Consistency	0.955	0.975	0.952	0.959	0.927	0.955
Background Consistency	0.949	0.948	0.957	0.975	0.973	0.974
Temporal Flickering	0.982	0.979	0.991	0.996	0.996	0.996
Motion Smoothness	0.984	0.977	0.985	0.984	0.979	0.984
Dynamic Degree	0.775	0.803	0.744	0.633	0.619	0.597
Aesthetic Quality	0.644	0.576	0.624	0.656	0.644	0.653
Imaging Quality	0.684	0.634	0.664	0.663	0.619	0.659
Object Class	0.966	0.957	0.950	0.946	0.921	0.930
Multiple Objects	0.872	0.814	0.850	0.851	0.791	0.862
Human Action	0.966	0.910	0.934	0.960	0.966	0.972
Color	0.853	0.930	0.874	0.883	0.872	0.879
Spatial Relationship	0.774	0.798	0.739	0.779	0.735	0.795
Scene	0.548	0.509	0.563	0.568	0.515	0.569
Appearance Style	0.200	0.220	0.199	0.217	0.218	0.217
Temporal Style	0.244	0.234	0.236	0.248	0.243	0.248
Overall Consistency	0.266	0.254	0.261	0.270	0.264	0.269
Quality Score	0.846	0.828	0.843	0.846	0.827	0.841
Semantic Score	0.800	0.793	0.788	0.810	0.785	0.812
Total Score	0.837	0.821	0.832	0.839	0.819	0.835

Table 10 Extended VBench scores from Table 2 for Wan2.1-1.3B (base 50-step and distilled 4-step models) for dense attention as well as trained VSA and MONARCHRT.

Metric	Dense Attention	SVG (85% sparse)	RadialAttention (85% sparse)	Exact top- k (85% sparse)	MONARCHRT (90% sparse)
Subject Consistency	0.959	0.855	0.970	0.942	0.949
Background Consistency	0.960	0.935	0.963	0.935	0.954
Temporal Flickering	0.990	0.972	0.993	0.985	0.986
Motion Smoothness	0.985	0.976	0.988	0.981	0.983
Dynamic Degree	0.653	0.097	0.539	0.806	0.753
Aesthetic Quality	0.650	0.398	0.632	0.595	0.643
Imaging Quality	0.680	0.608	0.701	0.675	0.698
Object Class	0.946	0.026	0.846	0.809	0.963
Multiple Objects	0.859	0.004	0.718	0.558	0.878
Human Action	0.966	0.084	0.808	0.748	0.960
Color	0.872	0.848	0.897	0.916	0.880
Spatial Relationship	0.776	0.022	0.817	0.683	0.829
Scene	0.580	0.000	0.319	0.213	0.563
Appearance Style	0.205	0.206	0.192	0.199	0.196
Temporal Style	0.244	0.035	0.235	0.224	0.241
Overall Consistency	0.265	0.047	0.244	0.234	0.264
Quality Score	0.844	0.715	0.841	0.834	0.847
Semantic Score	0.804	0.214	0.718	0.658	0.808
Total Score	0.836	0.615	0.816	0.799	0.839

Table 11 Extended VBench scores from Table 3 for Self-Forcing, comparing dense attention, several sparse baselines, and MONARCHRT all in a training-free setting. For RadialAttention and SVG, the first denoising step (out of 4 for Self-Forcing) and first attention block are retained as dense attention.

Metric	Dense Attention	SVG (85% sparse)	SVG2 (85% sparse)	SVG2 (90% sparse)	RadialAttention (85% sparse)	MONARCHRT (90% sparse)
Subject Consistency	0.955	0.901	0.946	0.934	0.832	0.952
Background Consistency	0.949	0.949	0.949	0.945	0.881	0.960
Temporal Flickering	0.982	0.976	0.986	0.985	0.979	0.991
Motion Smoothness	0.984	0.972	0.986	0.984	0.982	0.988
Dynamic Degree	0.775	0.853	0.742	0.742	0.361	0.653
Aesthetic Quality	0.644	0.526	0.623	0.598	0.539	0.622
Imaging Quality	0.684	0.532	0.654	0.625	0.545	0.686
Object Class	0.966	0.524	0.921	0.896	0.757	0.956
Multiple Objects	0.872	0.357	0.741	0.655	0.534	0.884
Human Action	0.966	0.900	0.952	0.928	0.954	0.964
Color	0.853	0.733	0.860	0.865	0.805	0.893
Spatial Relationship	0.774	0.376	0.669	0.654	0.463	0.821
Scene	0.548	0.231	0.537	0.510	0.408	0.549
Appearance Style	0.200	0.213	0.201	0.205	0.222	0.198
Temporal Style	0.244	0.202	0.238	0.234	0.236	0.240
Overall Consistency	0.266	0.218	0.264	0.260	0.252	0.263
Quality Score	0.846	0.792	0.837	0.824	0.738	0.841
Semantic Score	0.800	0.563	0.765	0.743	0.681	0.807
Total Score	0.837	0.746	0.823	0.808	0.727	0.834

Table 12 Extended VBench scores from Table 4 for 4-step distilled Wan 2.1-1.3B, comparing dense attention, several sparse baselines, and MONARCHRT all in a training-free setting.

C.2 Example Generations

We provide additional example generations for Self-Forcing and Wan in Figures 12 and 13 respectively. We use 5 prompts from MovieBench (Polyak et al., 2024) to generate videos for the dense model and MONARCHRT. The sample videos demonstrate that MONARCHRT can achieve comparable visual quality to the dense model.



"A detailed realistic photograph captures a German Shepherd gently placing a butterfly that landed on its nose onto a colorful flower..."

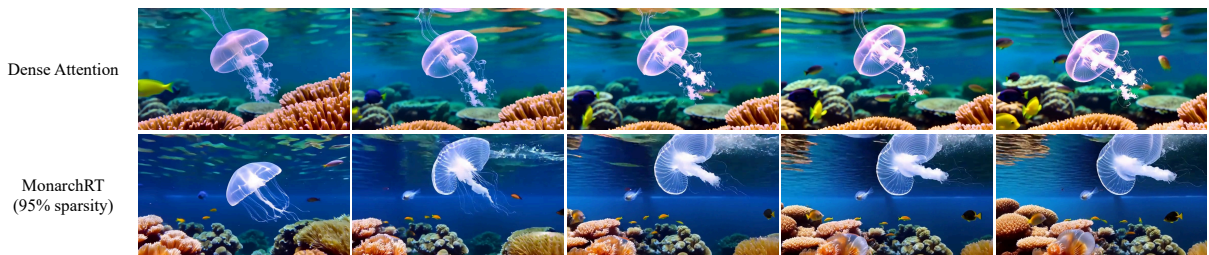


"A detailed landscape photograph capturing a majestic pedestal emerging from a meticulously tended flower bed..."

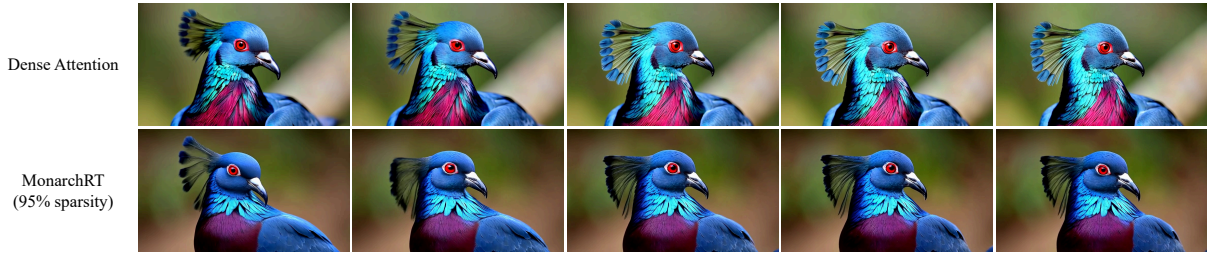


"An ultra-fast disorienting hyperlapse photograph capturing a car racing through a tunnel, transitioning into a chaotic labyrinth of rapidly growing vines..."

Figure 11 Example generations on Self-Forcing for exact top- k and MONARCHRT with 1 and 20 iterative refinement steps (training-free).



"A captivating underwater video showcasing a graceful jellyfish drifting through crystal clear water, its translucent tentacles flowing elegantly and..."



"A close-up shot of a Victoria crowned pigeon in a naturalistic wildlife photography style, showcasing its striking blue plumage and red chest..."



"A detailed photograph capturing a skilled gardener attentively planting seeds in a meticulously tended garden bed. The gardener, a middle-aged man..."

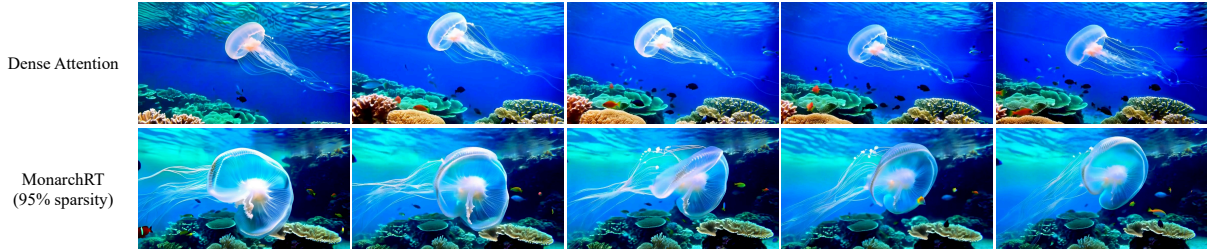


"A photorealistic closeup video of two pirate ships battling each other as they sail inside a steaming cup of coffee. The ships are intricately detailed..."

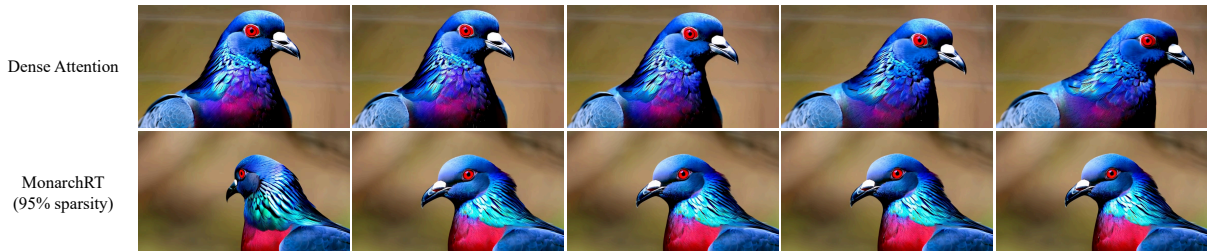


"A sci-fi action scene in a high-resolution digital art style, featuring an astronaut in a sleek, white space suit, fists raised, mid-air combat with a towering alien monster..."

Figure 12 Example generations for dense baseline and MONARCHRT (with 95% sparsity) on the same prompts for Self-Forcing.



"A captivating underwater video showcasing a graceful jellyfish drifting through crystal clear water, its translucent tentacles flowing elegantly and..."



"A close-up shot of a Victoria crowned pigeon in a naturalistic wildlife photography style, showcasing its striking blue plumage and red chest..."



"A detailed photograph capturing a skilled gardener attentively planting seeds in a meticulously tended garden bed. The gardener, a middle-aged man..."



"A photorealistic closeup video of two pirate ships battling each other as they sail inside a steaming cup of coffee. The ships are intricately detailed..."



"A sci-fi action scene in a high-resolution digital art style, featuring an astronaut in a sleek, white space suit, fists raised, mid-air combat with a towering alien monster..."

Figure 13 Example generations for dense baseline and MONARCHRT (with 95% sparsity) on the same prompts for Wan 2.1-1.3B (50-step bidirectional model).